Corrosion in Marine Structures

UNIVERSITY OF THESSALY

SCHOOL OF ENGINEERING

DEPARTMENT OF MECHANICAL ENGINEERING

Corrosion in Marine Structures

by

AIKATERINI GLYNOU

Submitted in partial fulfillment of the requirements for the degree of Diploma in Mechanical Engineering at the University of Thessaly

Volos, 2024

Corrosion in Marine Structures

Approved by the Committee on Final Examination:

Advisor	Dr. Gregory Haidemenopoulos, Professor, Department of Mechanical Engineering, University of Thessaly
Member	Dr. Eleni Kamoutsi, Lab Teaching Staff, Department of Mechanical Engineering, University of Thessaly
Member	Dr. Alexis Kermanidis, Associate Professor, Department of Mechanical Engineering, University of Thessaly

Date Approved: [Month dd, yyyy]

Acknowledgments.

I would like to express my gratitude to my supervisor, Professor Gregory Haidemenopoulos for inspiring me and for his assistance through the process of the composition of my thesis. Meanwhile, I would like to acknowledge all my professors who helped me build a strong background for my future career as a mechanical engineer. Last but not least I want to give my warm thanks to my family and friends who trusted and supported me all these academic years.

Corrosion in Marine Structures

Abstract

The scope of the current thesis is to address a very critical issue that significantly impacts the shipbuilding industry, which is corrosion on marine structures. Corrosion can provoke severe damage in ships, equipment, and constructions that are exposed to the seawater environment. Therefore, it is essential to study this topic in order to improve efficiency, maintain safe and environmentally responsible operations, and minimize expenses.

The study involved thorough bibliographic research on the marine environment and how it enhances the corrosion mechanism. Furthermore, it presented the primary forms of corrosion that afflict marine structures along with methods used to mitigate and prevent the phenomenon. Additionally, a computational analysis using SolidWorks was conducted to calculate corrosion on a ship's hull by estimating the reduction in steel plating thickness.

The literature review revealed that the marine environment's high corrosiveness is influenced by factors such as salinity, temperature, oxygen concentration in the atmosphere and ocean water, sea depths, and water flow velocity. These factors provoke various corrosion types, but the main ones that appear more frequently in maritime are atmospheric corrosion, flow-accelerated corrosion, erosion-corrosion, cavitation, and galvanic corrosion. Moreover, the simulation process indicated that the decrease in thickness due to corrosion leads to increased stresses on the ship, thereby compromising its structural integrity.

Hence it is crucial to implement techniques in order to eliminate this problem and ensure safety and enhance the ship’s longevity. Therefore, corrosion must be carefully managed from the initial design phase, but also throughout its operation, through regular inspections and maintenance.

Corrosion in Marine Structures

Περίληψη

Ο σκοπός της παρούσας διπλωματικής εργασίας είναι η αποτύπωση ενός μείζονος ζητήματος που προσβάλει τη ναυπηγική βιομηχανία, το οποίο είναι η διάβρωση των θαλάσσιων κατασκευών. Η διάβρωση μπορεί να προκαλέσει σημαντική υπονόμευση σε κατασκευές, εξοπλισμό και πλοία εκτεθειμένα σε θαλάσσιες συνθήκες. Συνεπώς, είναι απαραίτητη η μελέτη αυτού του θέματος έτσι ώστε να βελτιστοποιηθεί η απόδοση, να επιτευχθούν ασφαλείς και οικολογικές λειτουργίες, αλλά και να ελαχιστοποιηθούν οι δαπάνες.

Η μελέτη περιλαμβάνει διεξοδική βιβλιογραφική ανασκόπηση στο θαλάσσιο περιβάλλον και πως αυτό ενισχύει τους μηχανισμούς της διάβρωσης. Επιπλέον, παρουσιάζονται κυρίαρχες μορφές διάβρωσης που υποβαθμίζουν τις ναυπηγικές κατασκευές. Παράλληλα, προτείνονται μέθοδοι για την άμβλυνση του φαινομένου. Στη συνέχεια, έχει διεξαχθεί υπολογιστική ανάλυση χρησιμοποιώντας το λογισμικό SOLIDWORKS προκειμένου να εκτιμηθεί το ποσοστό διάβρωσης σε μία γάστρα ενός πλοίου, μέσω μείωσης των παχών των χαλύβδινων ελασμάτων.

Η βιβλιογραφική έρευνα αποκάλυψε ότι το ναυπηγικό περιβάλλον είναι ιδιαίτερα διαβρωτικό και επηρεάζεται από παράγοντες όπως την αλατότητα των υδάτων, την θερμοκρασία, την περιεκτικότητα της θάλασσας και της ατμόσφαιρας σε οξυγόνο, το βάθος στο οποίο βρίσκεται η κατασκευή και την ταχύτητα ροής του υγρού. Οι παράγοντες αυτοί πυροδοτούν διάφορες μορφές διάβρωσης. Οι πιο συχνές που εμφανίζονται στη ναυτιλία είναι η ατμοσφαιρική διάβρωση, η ροϊκά επιταχυνόμενη (FAC), η μηχανική διάβρωση, η σπηλαίωση, και η γαλβανική. Επιπρόσθετα, η διαδικασία της προσομοίωσης υπέδειξε ότι η μείωση των παχών εξαιτίας τη διάβρωσης, συντελεί στην αύξηση των τάσεων στο πλοίο και τελικά στην υποβάθμιση της στατικής ακεραιότητάς του.

Επομένως, είναι κρίσιμο να εφαρμοστούν τεχνικές με γνώμονα την καταπολέμηση του προβλήματος και την διασφάλισης της ασφάλειας και της μέγιστης διάρκειας ζωής. Οπότε, η διάβρωση πρέπει να διαχειρίζεται προσεκτικά από το αρχικό στάδιο του σχεδιασμού, αλλά και καθ' όλη τη διάρκεια της λειτουργίας του, μέσω τακτικών επιθεωρήσεων.

Contents

List of Figures

Corrosion in Marine Structures

Chapter 1: Introduction to Corrosion

1. Definition of Corrosion and Terminology

Corrosion is the natural interaction of a material (metal and its alloys, ceramics, polymers, and composites) with its reactive surroundings, which concludes with the altering of the material's properties. It is considered to be a complex electrochemical process and is affected by mechanical factors, such as strain, stress, external loads, the velocity of the fluid, surface structure, material construction, etc. Corrosion comprises a major cause of structural failure, due to the diminution of material that, in combination with mechanical forces, might lead to its operation degradation or fracture. [1], [2]

Corrosion is characterized as an electrochemical phenomenon due to the existence of electrical current during the chemical reaction. The main elements that distinguish electrochemical corrosion are: the anode, the cathode, the electrolyte, and the metallic path. [49]

The anode is the region of the metal where atoms of the metal are converted into ions, causing the metal to dissolve in the electrolyte. The produced electrons pass through the anode and the metal conductor to the cathode. Corrosion and metal loss occurs in the anodic state, where oxidation takes place. The amount of current flow is correlated with the quantity of metal that will corrode.

The cathode is the part of the metal where electrons are consumed. A reduction reaction takes place at the cathode. Oxidation and reduction are simultaneous phenomena.

The electrolyte is the ion conductor that allows the transportation of ions between the anode and the cathode.

The metallic path is the connection between the anode and the cathode, and the path for electric current flow. It facilitates the transportation of electrons, that were generated at the anode, to the cathode.

A typical example of an electrochemical reaction is the phenomenon between two different plates, one from copper and one from iron, placed into seawater. Their edges are connected with a metal wire outside the water. Thus, seawater acts as an electrolyte, since it converts the chemical energy of actions into electrical energy. As a result, an

electric current is generated and it flows through the metal plates. This interaction, known as electrolysis, leads to corrosion of the metal surface.

1.2 Impact of Corrosion

The consequences of corrosion are various, and they have a large extent, so research into its mechanisms is critical. Furthermore, a significant amount of metals and alloys (40%) are destroyed annually due to corrosion. These implications can be divided into three aspects, economy, energy saving, and environmental and human safety. [1,2,5]

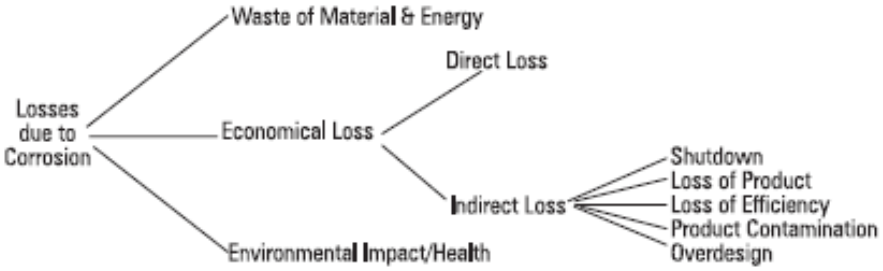

Figure 1. 1 Classification of Corrosion losses

1.2.1 Economic Impact of Corrosion

The significance of the cost due to corrosion was conceived in 1950. Since then, various studies have taken place in order to eliminate this expense. According to the International Measures of Prevention, Application, and Economics of Corrosion Technologies (IMPACT), the estimated cost of corrosion, globally, is US$2.5 trillion, which represents 3.4% of the gross domestic product (GPD) in 2013. This amount does not include expenses that are associated with human safety, environmental consequences, or product loss. In order to determine the actual global expenditure of corrosion, Nace IMPACT included various studies, like India 2011-2012, the United States 1998, Japan 1997, Kuwait 1987, and the United Kingdom 1970. Conclusions were made by separating the economy into three economic sectors, Agriculture, Industry, and Services, and also five geographic regions. Lastly, considering the cost of corrosion (CoC) of each region, the GPD, and dividing it by the economic sector, the financial breakdown was defined, in Table 1. [3]

Table 1 Global Cost of Corrosion by Region by Sector (Billion US$ 2013) [3]

Economic Regions	Agriculture CoC US$ billion	Industry CoC US$ billion	Services CoC US$ billion	Total CoC US$ billion	Total GDP US$ billion	CoC % GDP
United States	2.0	303.2	146.0	451.3	16,720	2.7%
India	17.7	20.3	32.3	70.3	1,670	4.2%
European Region	3.5	401	297	701.5	18,331	3.8%
Arab World	13.3	34.2	92.6	140.1	2,789	5.0%
China	56.2	192.5	146.2	394.9	9,330	4.2%
Russia	5.4	37.2	41.9	84.5	2,113	4.0%
Japan	0.6	45.9	5.1	51.6	5,002	1.0%
Four Asian Tigers + Macau	1.5	29.9	27.3	58.6	2,302	2.5%
Rest of the World	52.4	382.5	117.6	552.5	16,057	3.4%
Global	**152.7**	**1446.7**	**906.0**	**2505.4**	**74,314**	**3.4%**

The economic defects caused by corrosion can be divided into direct and indirect. The first one appertains to the replacement cost of the structure or its part, that has sustained corrosion, to the essential inspections, and the expenses for maintenance, such as sustainable paints and anticorrosion coatings, and cathodic protection. The indirect cost is estimated to be almost equal to the immediate (4% of GPD) and is linked to the lost time, due to an unexpected shutdown of an operation or a machine, until the damage is restored. Moreover, corrosion can militate loss of material or pollution of an establishment that does not conclude to its failure, but to the mitigation of the efficiency of its function. A distinguishing example is the pitting of a ship's hull, which increases the surface -asperity, and concurrently, decreases the velocity of the ship to 7-14% annually. The outcome of this fact is the radical rise in fuel expenses and finally labor costs. Last but not least, manufacturing companies tend to overdesign a structure in order to deter the loss of material, which causes additional expenses to an industry. [1,4,5].

In the maritime industry, the international cost of corrosion is estimated to be $80 billion, annually, while 40% of this amount is accountable for coatings and conservation (direct cost). [6]

1.2.2 Energy saving

The waste of energy is solely connected to the amount needed to manufacture metals. Furthermore, surveys have shown that every 90 seconds, one ton of steel becomes rust, while the demand for energy to cover this loss approaches the average energy consumption of a family, in three months. A distinguished example is the fact that ¼ of the global Ferrum production, which is approximately 150 million tons annually, is

destroyed due to corrosion, and simultaneously, 50% of each ton produced, is used for the replacement of corroded steel. [1,7]

1.2.3 Environmental and Human Safety Impact of Corrosion

When a failure of construction occurs, it can lead to devastating results for the environment. Specifically, there is a high risk of leakage of harmful substances that can cause pollution in the air, the sea, forests, and other natural sectors. In the marine industry, for example, numerous oil spills have happened with thousands of tons of oil spilled into the sea, leading to the complete destruction of flora and fauna of the area. Apparently, these kinds of accidents derogate the safety of the workforce and the general public. There are various cases where these incidents have provoked the undermining of the quality of life, have caused serious injuries, and sometimes, they were fatal. [5]

In conclusion, the damage caused by corrosion can be really expensive, thus it is sensible for industries and authorities to invest their money in corrosion protection, for the purpose of preventing damages that can result in failure, a shutdown of an operation, and accidents that erode human and environmental safety.

Chapter 2: Marine Environment

There are various factors that contribute to the corrosiveness of the marine environment and can cause significant damage to marine structures, ships, and other equipment that are exposed to seawater. These factors are; the salinity of ocean water due to the high concentration of dissolved salts, oxygen which mainly causes the oxidation of metals, the temperature and pH of the water, marine organisms, currents, and the flow velocity, and lastly, the depth. They provoke the initiation of cracks, pits, grooves, crevices, and eroded parts.

2.1 Salinity

Salinity is a crucial factor in the corrosion of metals in the marine environment. The average concentration of dissolved salts in seawater is about 3.5%. The predominant composites are sodium and chloride ions. Chlorine ions empirically determine the water's salinity (1.80655 * Cl^-). However, the actual amount of salinity can be calculated by measuring the conductivity of the water, which translates to its ability to conduct electric currents. This measurement can be obtained by considering the different dissolved salts that compose ocean water. The higher the concentration of these salts, the greater the conductivity of the water. According to experiments conducted in artificial seawater (ASTM D1141-98), the approximate quantity of these salts is shown in Table 2. [8]

Table 2 Artificial Ocean water composition according to ASTM D1141-98 (2013)

	Salt concentration [g/dm^3]	Salt [%]
NaCl	24.53	0.681
$MgCl_2$	5.2	0.144
Na_2SO_4	4.09	0.114
$CaCl_2$	1.16	0.0322
KCl	0.695	0.0193
$NaHCO_3$	0.201	0.00558
KBr	0.101	0.00280
H_3BO_3	0.027	0.000749
$SrCl_2$	0.025	0.000694
NaF	0.003	0.0000833
$Ba(NO_3)_2$	0.0000994	0.00000276
$Mn(NO_2)_2$	0.000034	0.000000944
$Cu(NO_3)_2$	0.0000308	0.000000855
$Zn(NO_3)_2$	0.0000096	0.000000266
$Pb(NO_3)_2$	0.0000066	0.000000183
$AgNO_3$	0.00000049	0.0000000136

Electricity is conducted when sodium chloride (NaCl) decomposes and produces Na+ and Cl^- ions. The chloride ions penetrate the surface of the metal and destroy the passive film, especially if there is a pre-existing scratch on the ship's hull. This destruction is caused due to the bonds they form with metals ($M^+ + Cl^- \rightarrow MCl$). When this chemical compound is exposed to water, hydrolysis occurs which leads to the formation of hydrochloride ($MCl + H_2O \rightarrow MOH + HCl$). The low pH (pH < 7) of the HCl acidifies the environment and makes it significantly corrosive. In addition, these reactions cause the generation of anodic and cathodic areas with different electronegativity and thus, cause the rapid movement of electrons that accelerate the rate of corrosion. (Figure 2.1) [2], [9]

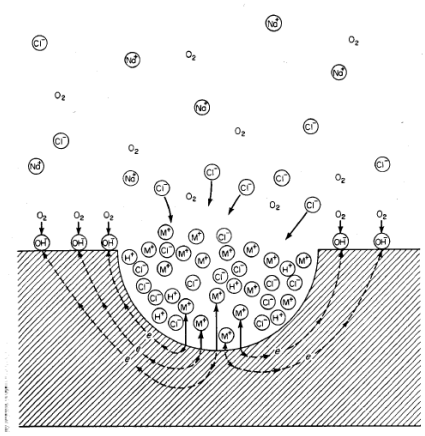

2. 1 Surface destruction and electrons movement

The value of salinity varies, depending on several factors. Different areas have different local salinity, initially due to the temperature and consequently the evaporation of the ocean water, which causes the increase of the salt concentration. Moreover, water exchange from ocean currents and the runoff from rivers and streams can transport water with higher or lower salinity, affecting the overall salinity of seawater in different regions. Finally, when the sea freezes, it adds to the water's dissolved solids and salt, and when it liquefies there is a rise of freshwater and therefore a reduction of salinity levels.

A typical example of low salinity is the Baltic Sea, because of the variety of sweet water inflows from rivers, streams, and melting ice. In addition, there is a limited ocean water exchange since the only passageway for water transportation is through the narrow Danish straits. Also, as a result of the low temperature in the area, the rate of

evaporation is significantly low. Hence, the Baltic Sea is considered moderately salinized, mainly in areas close to freshwater inputs. [9]

However, the corrosion rate of carbon steel reaches the maximum amount when the concentration of sodium chloride is 3.5%. After that value, the rate tends to mitigate (Figure 2.2), because of the rapid decrease of dissolved salt content, below 4 which is the limit of the operating conditions. For example, it is observed that in the Salton Sea, the content of dissolved salts is really low (2-4 mg/L), which is the condition of hypoxia, while in the Dead Sea, the content is 0.1mg/L, which translates to anoxia.[10]

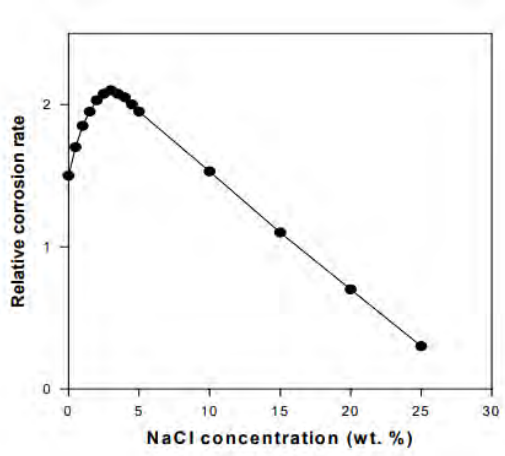

Figure 2. 2 Effect of salt concentration on the corrosion rate

2.2 Oxygen Concentration

The concentration of dissolved oxygen in saltwater can significantly affect the corrosion rate of metals immersed in the water. Oxygen is a fundamental component in the electrochemical reactions that lead to corrosion, and its presence in water can influence the rate of these reactions. In general, the concentration of dissolved oxygen in seawater increases the rate of metal corrosion. This happens because oxygen reacts with the metal surface to generate metal oxides or other compounds, weakening the metal and increasing its corrosion rate. When the content of dissolved oxygen is below a certain value, a protective film is formed at the metal surface which mitigates the corrosion rate. However, as the content increases, the film becomes unstable, so the oxygen is diffused through the surface of a metal which leads to the rise of the corrosion rate of the steel. [12]

During the diffusion, the cathodic reaction (reduction of oxygen) occurs, where the electrons that were produced at the anodic reaction (oxidation), are now consumed in order to form hydroxide (OH^-). [12], [2] (Figure 2.3)

$$Oxidation: \ M \rightarrow M^{n+} + ne^- \ or \ Fe \rightarrow Fe^{2+} + 2e^-$$

$$Reduction\ of\ Dissolved\ Oxygen: \quad O_2 + 2H_2O + 4e^- \rightarrow 4OH^-$$

$$Chemical: \quad 2Fe + 2H_2O + O_2 \rightarrow 2Fe(OH)_2$$

The iron hydroxide does not provide protection to the steel surface; rather, it enables exposure to the atmosphere, leading to further oxidation and the formation of rust.

$Chemical: \quad 4Fe(OH)_2 + 2H_2O + O_2 \rightarrow 4Fe(OH)_3$ [2]

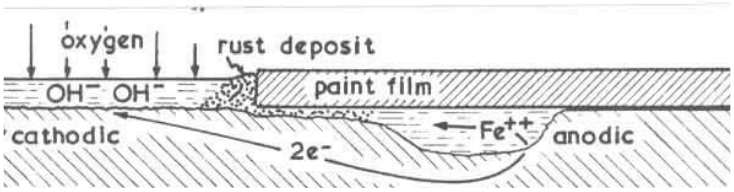

Figure 2. 3 Corrosion mechanism due to oxygen

The impact of dissolved oxygen is affected by the pH of the surrounding environment, temperature, and salinity. Nevertheless, the primary factor which is directly correlated with oxygen is the seawater temperature.

For steady water temperatures, a study conducted by Melchers indicates that the function between corrosion loss and dissolved oxygen is relatively linear. The experiment was concluded after one year and the samples were placed at 45m depth at temperatures of 7ºC, 19 ºC, and 29 ºC. In Figure 2.4 the data from the study are presented and it is evident that dissolved oxygen content has a linear correlation with the metal degradation. Meanwhile, the study revealed that oxygen concentration and temperature have an equivalent relation, since as the temperature increases so does the dissolved oxygen. [16]

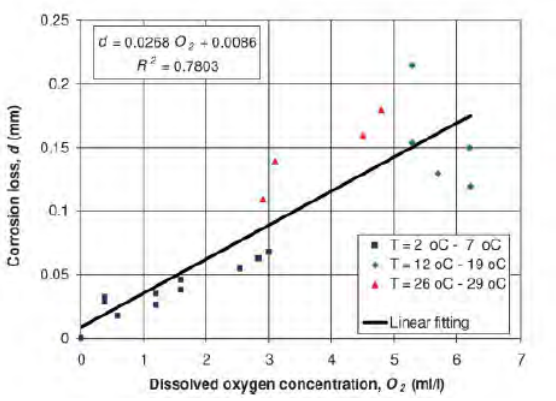

Figure 2. 4 Corrosion loss and dissolved oxygen concentration correlation after 1 year

2.3 Water flow velocity

One of the most crucial factors in the initiation of corrosion is the flow rate. At high velocity, there is a significant increase in erosion and therefore mechanical wear of the material. Even in low flow rates, mechanical fracture occurs while the passive film of oxides is affected by the velocity of the fluid, but the damage can be sprung back, due to the re-passivation property of the film and the transportation of oxygen through the flow. However, beyond the critical value of each material, there is not enough time for this property to operate, while anodic and cathodic areas are created, resulting in the acceleration of the corrosion effect. (Figure 2.5) [13]

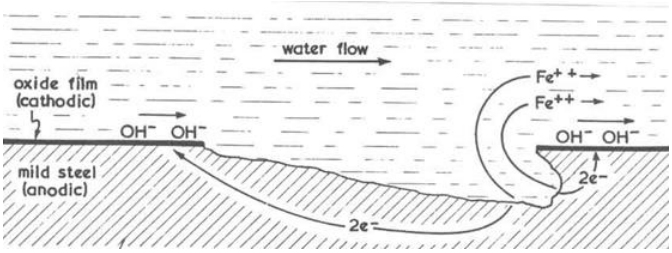

Figure 2. 5 Damage of the passive film

Carbon steel is the most common steel used in marine engineering due to its inexpensive cost and great mechanical strength. However, carbon steel has a low content of nickel and chromium which causes the inability to form a protective film on the surface and thus results in the deterioration of the material in the corrosive conditions of seawater. Moreover, seawater in contact with the steel material is constantly moving because of the speed of the vessel, water, and wind currents, leading to the generation of flow accelerating corrosion and erosion corrosion. Apparently, the

phenomenon is more frequent in high-speed vessels, since the speed rises above the critical value of 8-10m/s. [14]

There is a vast difference between carbon steel behavior in seawater and pure fresh water. In fresh water, the passive film can be created on the surface of the metal. Particularly, an initial increase in fluid velocity can cause the rise of corrosion rate, while oxygen molecules are transferred to the surface, but when the flow rate is high, the concentration of oxygen enables the generation of a protective film. Conversely, carbon steel in ocean water is unable to establish passivity at any velocity, because of the immense quantity of chloride ions, hence the corrosion rate tends to rise while the flow rate increases. Corrosion products such as rust layering and marine fouling, operate as corrosion protection due to flow rate velocity. When this kind of coating is removed, the corrosion rate increases actively as the velocity of the fluid rises. Immersion tests, which are conducted in order to evaluate the progression of corrosion, have proven that the increased rate of corrosion is nonlinear, and it can be calculated through the exponential function of LaQue; [15]

$R^2 = 0.9989$ (Figure 2.6)

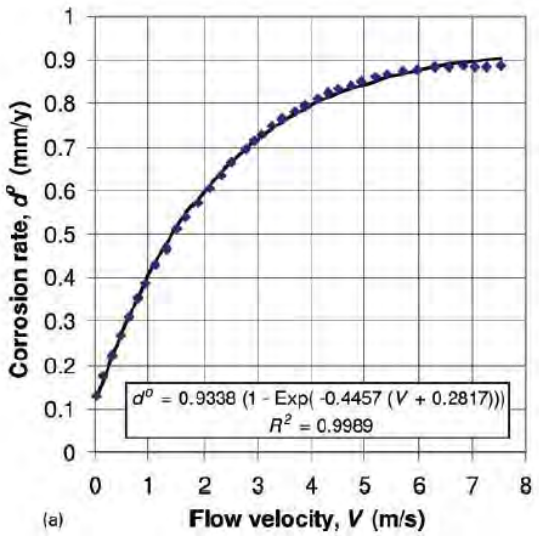

Figure 2. 6 Relation between corrosion rate on carbon steel and flow velocity

Furthermore, the ocean water stream transports sand and other abrasive particles that impinge on the steel surface and they can completely abase its passive film, reduce the thickness of the structure, provoke plastic deformation, and even initiate cracks. Thus, the erosion mechanism is enhanced and accordingly, the corrosion process is accelerated.

Lastly, at high flow rates, when the fluid passes through areas of low pressure, bubbles, and cavities are generated and collapse with the rise of the pressure. The shape of some marine applications causes the acceleration of the fluid's velocity and consequently, creates a local reduction of the pressure (Figure 2.7). The bubble collapse is capable of the destruction of the oxidation film of the material. This phenomenon is cavitation, and it is a form of erosion-corrosion that is a serious threat to the marine industry. [16]

Figure 2. 7 Bubbles formed at the edges of the propeller, where the velocity is highest.

2.4 Temperature

The ocean temperature range is proven to be about -2^{o}C at the poles and it can reach up to 40^{o}C at the tropics, whilst the mean value is 3.5^{o}C. Seawater temperature can considerably affect the rate of metal corrosion in numerous ways. According to Melchers's research, the relation between the corrosion rate and the temperature appears to be almost linear. Higher temperatures typically hasten the corrosion mechanism because they accelerate the chemical reactions, increase the kinetic energy of the sea molecules, alter the properties of the water, influence the microbial activity, and lastly, cause water evaporation, which enhances the water salinity.

Electrochemical reactions require the collision of reacting molecules in the appropriate direction and sufficient energy. Hence, the reactions are correlated with the kinetic energy. When the temperature rises, there is a rapid movement of water molecules, which allows the increase in the number of collisions and consequently leads to the acceleration of the chemical reactions between the steel and its environment. This phenomenon is described through the Arrhenius equation ($k= Ae^{-E/RT}$), where (k) is the reaction rate, (T) is the temperature, and (E) is the activation energy [21]. In addition, high kinetic energy facilitates a significant diffusion rate of dissolved oxygen and promotes the faster degradation of the metal. [18]

Dissolved oxygen content varies in different seawater temperatures (Figure 2.8). It is observed that as the temperature develops from 2°C to 19°C, the oxygen concentration is increased, as well as the corrosion rate, however, above that value, a small decrease is noted for both factors.

There has been a survey conducted by LaQue, where corrosion rate (d^0) as a function of the seawater temperature (T) is calculated, without considering, though, the effect of the marine microbial activity. In order to determine the accuracy of the predicted data and the actual response of the variables, a factor R^2 is used, which ranges between 0 and 1. As R approaches the value 1, the accuracy increases. The plots (Figure 2.9) were made from the following equations. [19]

$$d^0 = 0.0014 * T + 0.0154 \ (T \ in \ C^o)$$
$$d^0 = 0.0014 * T - 0.3708 \ (T \ in \ K)$$

Accordingly, it is clearly distinguishable that higher temperatures provoke faster corrosion behavior, whilst it is notable that the corrosion rate of the steel at 25 °C is almost double that of the one at 10 °C.

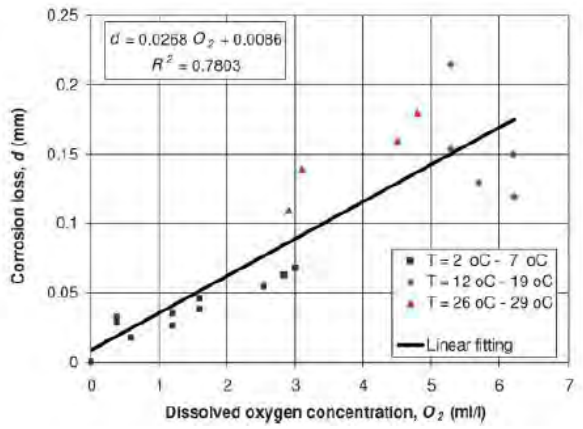

Figure 2. 8 Correlation of temperature, dissolved oxygen concentration and corrosion rate

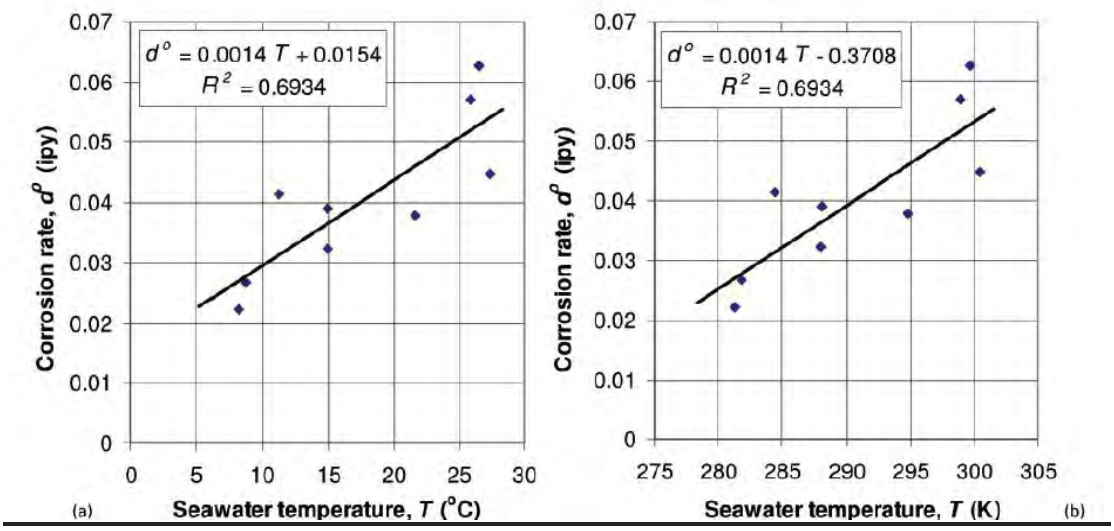

Figure 2. 9 Correlation between seawater Temperature and the Corrosion Rate

Furthermore, microbial-influenced corrosion is amplified through high seawater temperatures and can be simulated with the Arrhenius function. At immersion conditions, organisms form a microbial layer on the metal, which is known as biofilm, and can initiate pitting, under deposit and crevice corrosion. However, the activity of micro-organisms tends to deteriorate above a certain value of temperature, since they usually die at 35-40 ^oC [21], [20]. Finally, the bacterial generation as a function of temperature was calculated through an experiment that was published in FEMS Journals. A common method to measure the bacterial formation is by determining the incorporation of ^3H leucine. The different shapes on the plot (Figure 2.10) represent different seasons, winter, spring, and summer. In every case, there is low incorporation at low temperatures, up to 10 ^oC, thus low bacterial activity (, but there is a variation in the temperatures that cause the highest incorporation, depending on the season.) In winter, there is generally low bacterial production, with a maximum amount at 25 ^oC, in spring and summer, the incorporation is visibly increased, and the optimal temperature is 22 ^oC. Beyond this number, there is a rapid drop in the incorporation rate [21].

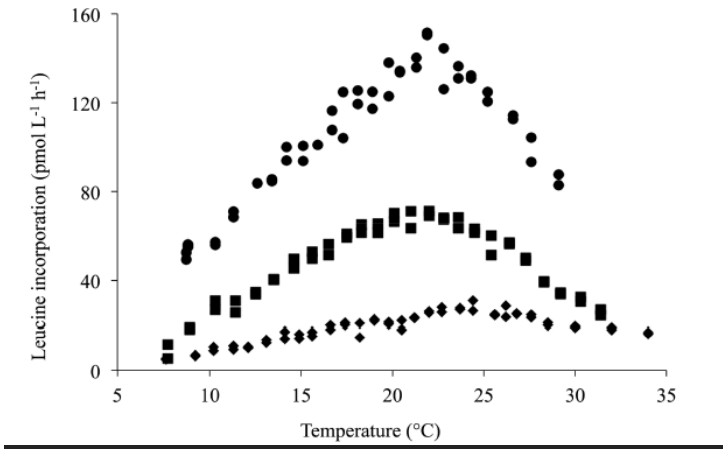

Figure 2. 10 H3 leucine incorporation at different seasons

2.5 Depth

Marine corrosion can be influenced by the immersion depth since it is relevant to the dissolved oxygen and chloride concentration, temperature, pressure, and flow velocities. Studies have been conducted on a carbon steel pipe pile in the Atlantic Ocean to evaluate the marine corrosion zones. There were found five different zones, relative to the immersion depth, which are; the atmospheric zone, the splash, the tidal, the immersion or submerged zone, and finally the sediment or subsoil zone. (Figure 2.11). [22]

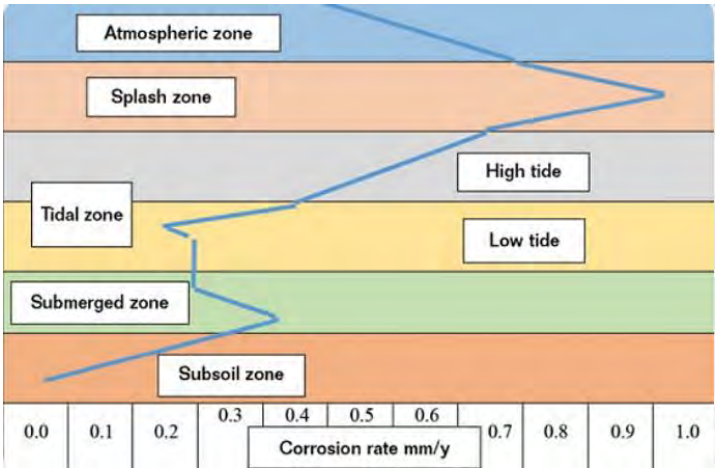

Figure 2. 11 Corrosion rate on different corrosion zones

- The atmospheric zone is 13m above the splash zone. It is observed that the corrosion rate increases as the sea level is approached, from 0.4mm/year to

0.7mm/year. This rise is caused by the NaCl solution which is enhanced close to the sea and by the saltwater drops and particles that are transferred by the wind and are deposited on the metal surface [22]. Finally, the atmospheric zone is characterized by pitting corrosion.

An experiment was conducted on four AISI 4135 steel coupons, placed in different depth areas in order to evaluate the corrosion on the four zones (atmospheric, splash, tidal, and immersion). The results from the visual inspection, after 3 months of exposure, were that the coupon at the atmospheric region formed a rust layer with no indication of fouling (Figure 2.12). When this layer was removed, small pits and grooves were found, which proves the existence of pitting corrosion [26].

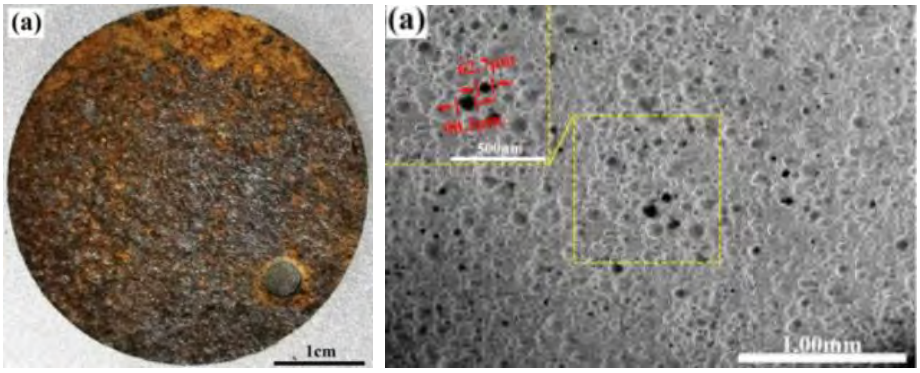

Figure 2. 12 (a1) Morphology of the rust layer on the coupon at the atmospheric zone (a2) pitting corrosion at the atmospheric zone

- The splash zone is considered to be the most threatening one for the steel since corrosion appears as localized and it is obvious that the highest corrosion rate is reached, 0.96 mm/year. This phenomenon occurs due to the large content of oxygen, where the ocean water collapses to the structure's metal surface, which deteriorates the coating and the passive film that operates as a corrosion protection method. [22]. This region is modular, and it can be determined through the correlation of the wave height, wind velocity, and direction. Moreover, the corrosion rate depends on the wetting and drying cycle. Consistently, during the drying process, the rate is amplified because of the remaining salt deposit on the steel as a result of the water evaporation [24].

  In the experiment, on AISI 4135 steel, the coupon at the splash zone, had major corrosion damage. Particularly, after the withdrawal of the rust film, the pits and the grooves were especially rough and deep [26]. (Figure 2.13)

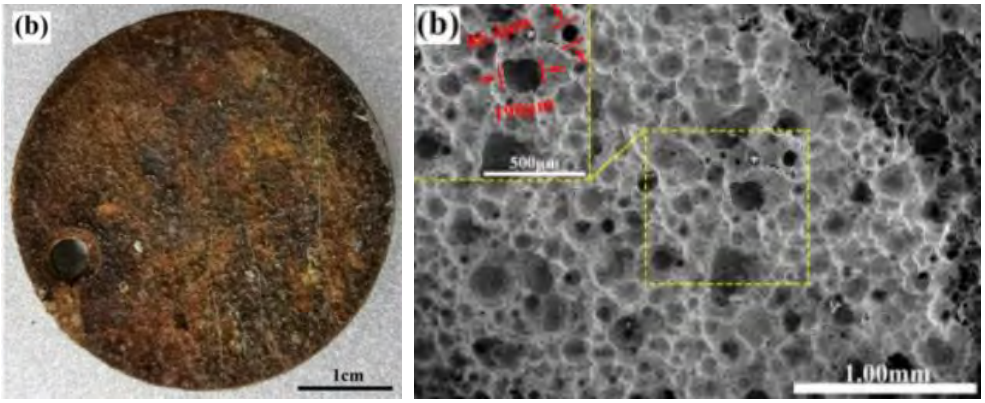

Figure 2. 13 (b1) Morphology of the rust layer on the coupon at the splash zone (b2) pitting corrosion at the splash zone

- The tidal zone can be divided into low-tide and high-tide regions. In the plot (Figure 10) it is stated that the corrosion rate is higher in the high tide area, however, research, from the Institute of Metal Research, in tidal zone corrosion proved that the degradation of the metal surface at the low tide region, is more severe. Corrosiveness is affected by several aspects, the chemical reactions, the oxygen concentration, the oscillation of the waves, the abrasion of floating particles and substances, and finally the microbial film on the steel. (Figure 2.14.c1) In this zone, the most common form of corrosion of the steel structure that appears is localized corrosion. (Figure 2.14.c2) The experiment was conducted on a wire-beamed electrode manufactured from Q235 steel, which is widely used in maritime. The electrode was tested in order to determine the different corrosion rates in the tidal zone. There were 20 different rows, where 1-4 applied to the atmospheric zone, 5-16 to the tidal zone, and 17-20 to the immersion zone. (Figure 2.15)

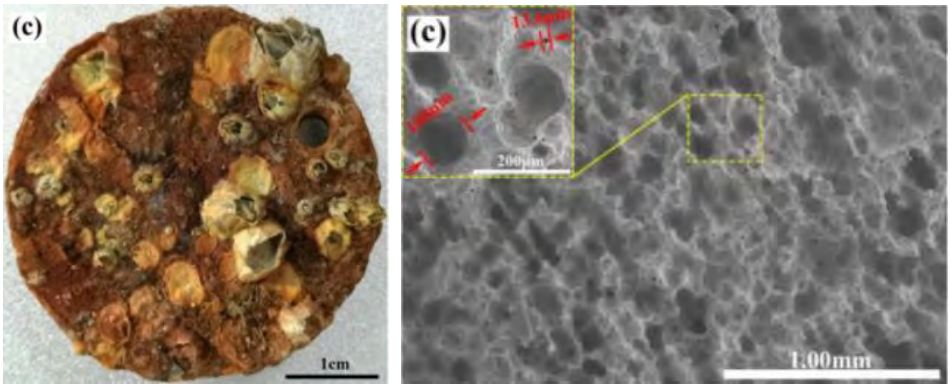

Figure 2. 14 (c1) The rust layer and biofouling film on the AISI 4135 coupon in the tidal zone, (c2) Localized corrosion in the tidal zone

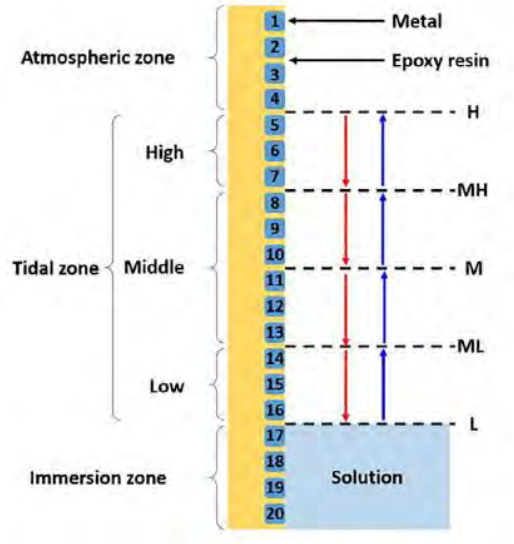

Figure 2. 15 The different corrosion zones on the electrode rows

It was observed that at the high tide, near the waterline, the dissolved oxygen content was increased, and the region acted as a cathode, whereas, below the middle tide area the anodic current density was gradually amplifying and became significantly high at the low tide area. (Figure 2.16)

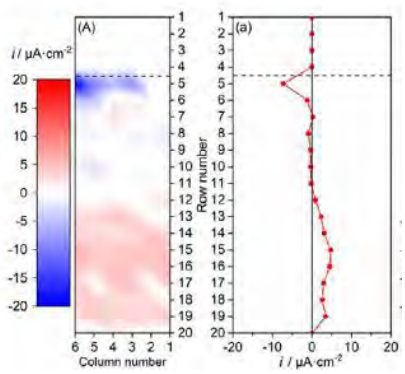

Figure 2. 16 (A) Density of anodic (red) and cathodic (blue) current (a) high tide and low tide region

After seven days, corrosion on the electrode surfaces was disguisable. Specifically, at the high tide zone, there was a yellowish rust layer over the surfaces with a small indication of metal diminution. Therefore, at the middle and especially at the low tide region corrosion is more severe as it gradually shows black spots on the rust film. The material loss from corrosion, which is equivalent to the anodic current density (i), was calculated through the equation:

$$\Delta h = \upsilon t = 3.27 * 10^{-3} * \frac{Mi}{n\rho} * \frac{t}{365}$$

Where Δh is the corrosion depth, (υ) the corrosion rate, (ρ) the steel density, (M) the molecular mass, and (n) the number of electrons.

In the plots (Figure 2.17), corrosion is displayed, in each zone and it is clear that the maximum metal degradation appears in the low tide zone with Δh=1.58*10-4*t1.02 in contrast to the high tide zone, with Δh=4.59*10-8*t1.77.

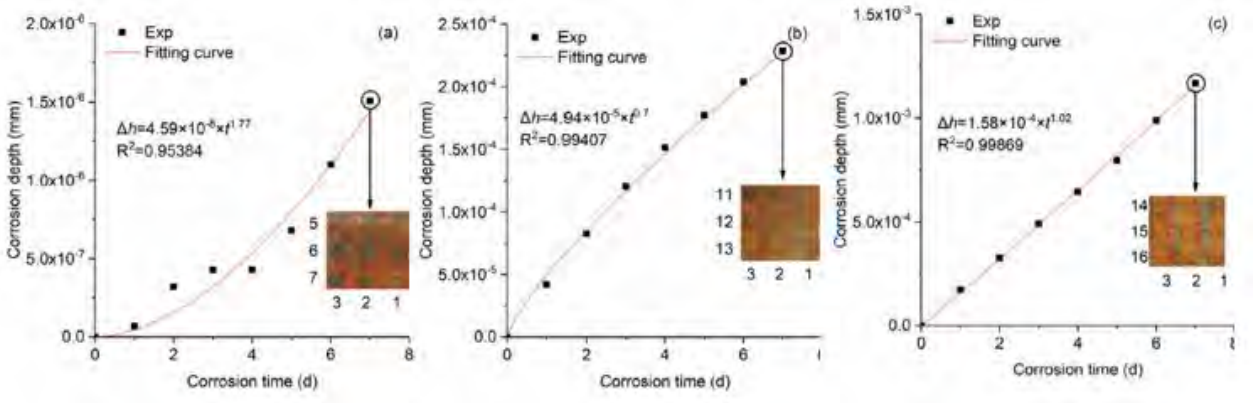

Figure 2. 17 Corrosion depth in (a) high tidal zone, (b) Middle tidal zone, (c) Low Tidal zone and the corroded electrodes in each zone

Hence, material loss due to corrosion is more significant at the low tidal zone, however, the inclination of the curve appears to be larger in the high tide region, which proves that the corrosion rate in this zone is eventually, higher [25].

- The immersion zone is the area where the structure is always at immersion conditions. [22] The most frequent form of corrosion that is observed is general corrosion and it is affected by oxygen concentration and the inhabitation of marine microorganisms on the steel surface.

  In the experiment on the AISI 4135 steel, the marine growth is easily evadable at the immersion area, however, the rust layer is less thick than the ones at the splash and tidal zones. After the removal of the outer film, the morphology of the sample surface is half smooth and the other half appears to be rough and has shallow grooves, which indicates the existence of general corrosion. Therefore, some small pits can be noticed, which are possibly caused by biofouling [26]. (Figure 2.18)

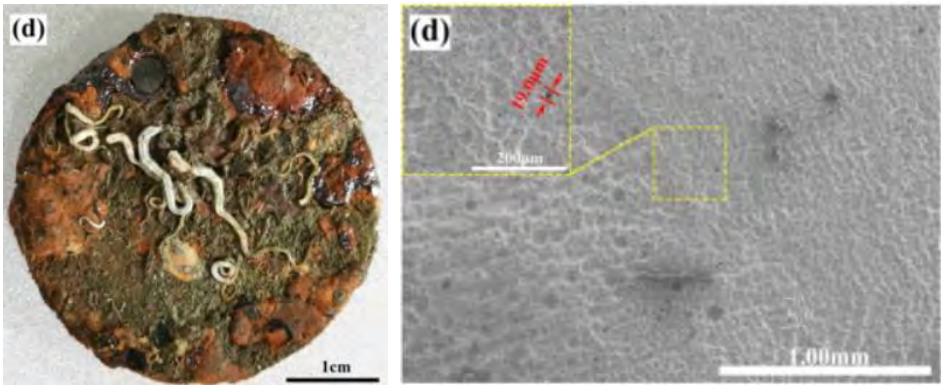

Figure 2. 18 (d1) Marine growth on the coupon in the immersion zone, (d2) General corrosion in the immersion zone

In the research on the Q235 steel wire beamed electrodes, corrosion was significantly high, and the experimental corrosion depth was measured to be Δh=1.67810-4*t1.15. This value is larger than the one in the tidal zone, due to the increased anodic current density in the submerged region (Figure 2.19). The rust layer was formed earlier than the other zones, and there were dark and dense rust surfaces on the electrode. Therefore, the corrosion rate in this area is relatively low over time, in contrast with the atmospheric and splash zones.

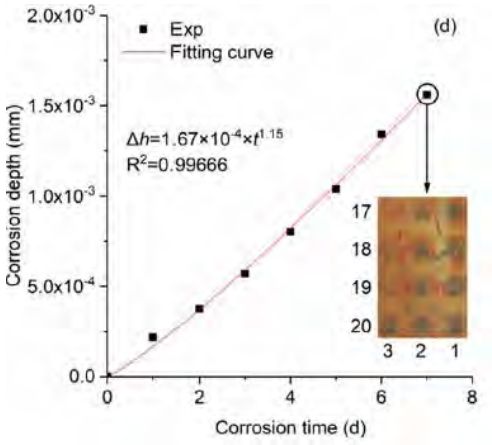

Figure 2. 19 Corrosion depth in the immersion zone and the corroded electrode

Chapter 3: Types of Corrosion in the marine environment

Corrosion in Marine Structures

Marine structures and vessels suffer from various mechanisms of corrosion, which can cause weakness and degradation of the steel structure and can lead to fracture. The principal forms of corrosion that appear in the shipping industry are atmospheric corrosion, galvanic, microbial, flow-accelerated corrosion (FAC), erosion corrosion, and cavitation. Meanwhile, the main areas of the ship that corrosion attacks are the hull, the shell and deck plating, the stiffeners, the hatch covers or cargo hatch, the side frames, the watertight bulkheads, the ballast, and oil tanks, and finally the heat exchangers of the ship's engine. [29]

3.1 Atmospheric Corrosion

Carbon Steel corrodes at a different rate, depending on the atmosphere and the relative time at which it is exposed. Thus, it is important to consider Atmospheric corrosion, which occurs when a steel surface interacts with the atmosphere, without seawater immersion conditions. Therefore, humidity initiates corrosion by forming a thin aqueous layer on the metal, which operates as the electrolyte layer and it allows the anodic and cathodic reactions to take place [30]. (Figure 3.1)

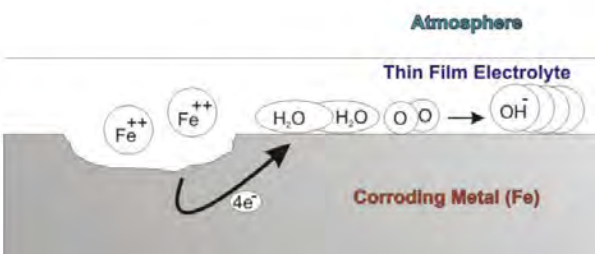

Figure 3. 1 The electrolyte film on the metal

According to the previous chapter, the atmospheric zone is highly corrosive due to the seawater drops and particles transferred from the wind that contain sodium chloride solution and other corrosive chemical components such as oxygen, chloride ions, and pollutants like sulfur oxides. These composites vary from different regions and the synergy of humidity and temperature determines the level of corrosion. When the moisture layer on the steel surface is enhanced with sulfur oxides and chlorine deposits, the damage is exacerbated [30].

3.1.1 Regions of the ship exposed to atmospheric corrosion.

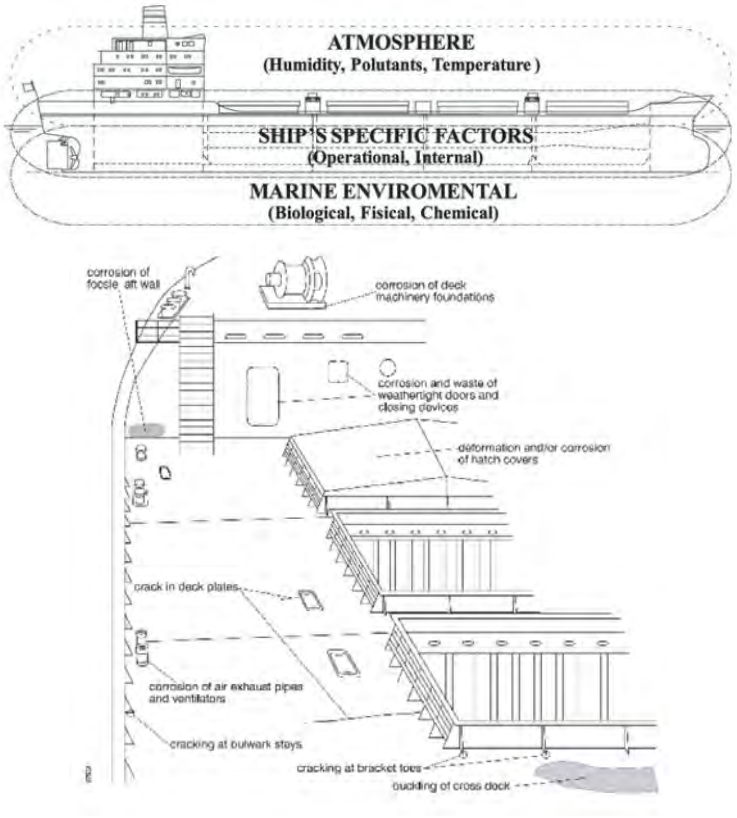

Figure 3. 2 [33], [35] Factors influencing the corrosion of ship structures.

The main areas of the ship that are prone to atmospheric corrosion are: (Figure 3.2)

- The upper area of the hull is subjected to the action of the aggressive atmospheric environment that has a high concentration of chlorides, oxygen, and other corrosive elements such as pollutants, while additionally receiving the incidence of seawater aerosol transferred by the wind and the waves. This area is also possessed by relative humidity, which forms a small wet layer that with the effect of pollutants and chlorides, acts as an electrolyte and corrodes the structure.
- The upper deck, which is the topmost deck of the ship, is vulnerable to rain precipitation, condensation due to the breaking waves, and severe humidity. In addition to the environmental factors that destroy the steel plating of the deck, the irregular geometry of the deck with welded plating, hatch covers, manholes, and other structures, can cause stress concentration and accelerate corrosion (Figure 3.2). [35]
- The superstructure which is the additional construction to the upper deck and is where the bridge is located as well as the accommodations. (Figure 3.3) This

structure is manufactured usually from steel and aluminum which can be easily corroded.

- Pipes and fittings from water ballast tanks, oil tanks, and ventilation pipes, which are located outside, at the upper deck (Figure 3.3), are liable to corrosion. They are mainly manufactured by copper-nickel alloys and carbon steel. If they are severely corroded, seawater might permeate into the tanks and contaminate the fuel, damage the tanks, and even afflict the ship's stability [35].

Figure 3. 3 Exterior piping and fittings

- Mooring, towing, and anchoring equipment are directly exposed to the corrosive marine environment, which acts simultaneously with the mechanical stresses that apply to this equipment and damage it severely. The equipment used for the mooring mechanism is a collection of fittings and systems on a ship (Figure 3.4) that is utilized to secure and anchor the ship while it is tied at a pier, to buoys, or alongside another vessel. The systems include capstan and winches that operate to control the mooring lines, namely the ropes and the steel chains [36]. Towing equipment is used in shipping to encompass pushing, towing alongside, and pulling a vessel or object with a towline (Figure 3.4). Both dynamic and static towing are possible in towing operations. The main mechanism involved in towing is the winch which determines the tension of the ropes and towing cables, which can be prone to the atmospheric corrosion [37].

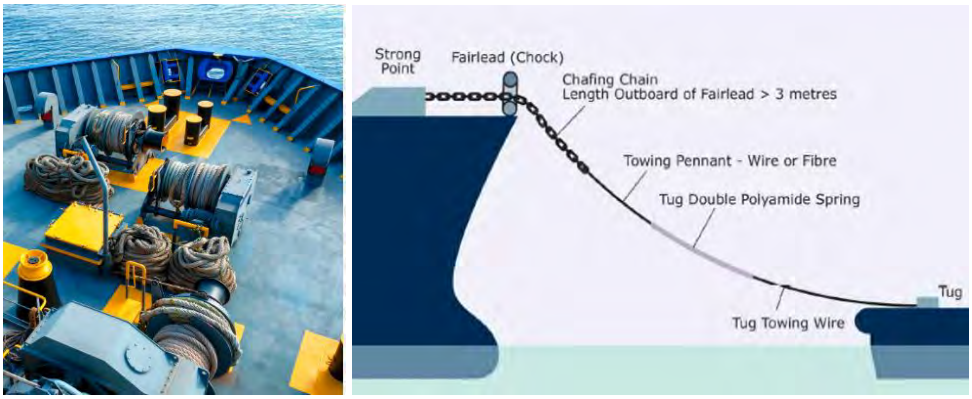

Figure 3. 4 Left, mooring equipment, right towing arrangement.

- Rigging for sailing vessels which includes mast and ropes are structures that support the sails. Masts are made from aluminum and the most frequent form of corrosion that occurs is galvanic due to their contact with steel brackets and fittings on the base. Galvanic corrosion is enhanced by the presence of sea spray and the salinity of the marine atmosphere [38]. (Figure 3.5)

Figure 3. 5 Galvanic Corrosion on a mast that appears as bubbles.

- Ballast tanks, cargo tanks, and cargo holds suffer from intense damage from corrosion because of the corrosive behavior of their load such as seawater, fuel, crude oil, and bulk cargo. However, they are prone to enclosed atmospheric corrosion when they are empty when an aqueous film is formed on their walls. In contrast with the surfaces that are exposed to the ocean air, these tanks are not influenced by the sun's radiation and precipitation, but by the time of wetness, salt deposit, and temperature. The salt deposition varies in different empty holds spaces, and it might depend on the previous cargo or on washing with saltwater. For example, in cargo holds there can be remnants of coal, and in ballast tanks seawater. Furthermore, the duration of wetness depends on the time of a single voyage since the tanks are reloaded and cleaned. Finally, humidity values are especially high in hold spaces, namely in the ballast tanks,

where the level of relative humidity reaches 90-100% when they are unloaded. [34]

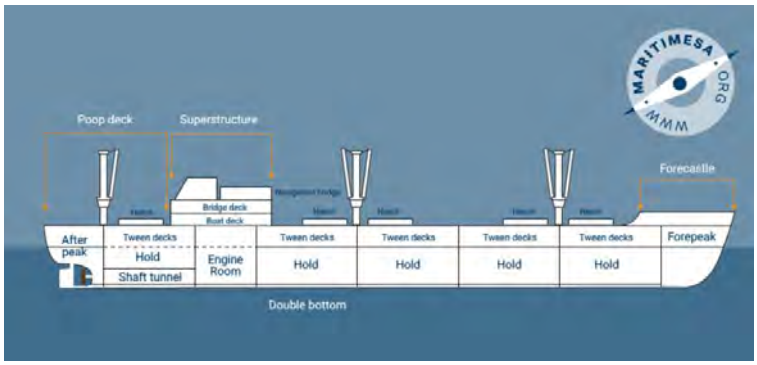

Figure 3. 6 Layout of a typical cargo ship

3.1.2 Sulfur oxide

Cargo and oil tanks contain hydrogen sulfide and sulfur dioxide and when they react with oxygen or the vapor water of the atmosphere, they form sulfurous acid, which is significantly corrosive. When the sulfurous acid comes in contact with the oxygen of the air, it produces sulfuric acid which is also a threat to the steel. [28], [30]

$$SO_2 + H_2O \rightarrow H_2SO_3$$

$$H_2SO_3 + \frac{1}{2}O_2 \rightarrow H_2SO_4$$

Sulfuric acid reacts with the metal, and it forms ferrous sulfate ($FeSO_4$), which appears at the steel surface initially as small nests, but as its concentration increases and the area is moist, a rust film covers the entire surface. The nests tend to collapse with the rise of pressure and accelerate corrosion [29]. (Figure 3.7)

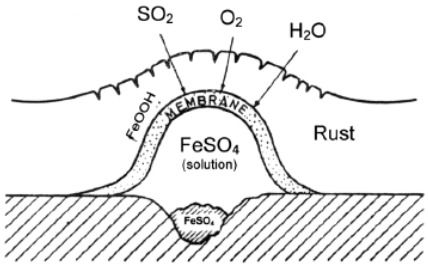

Figure 3. 7 Formation of FeSO4 nests and the rust layer

Moreover, the risk of corrosion increases during rain precipitation because the rainwater absorbs the sulfur dioxide which provokes acid rain. Hence, the pH of the water decreases, and the degradation of the metal is escalated. This phenomenon is

proven through simulating tests conducted on A3 carbon steel, with rainwater at different pH values (3.4, 4.5, 5.7). The corrosion damage was evaluated by the metal weight loss, and it seems to increase with the reduction of the pH of the rainwater (Figure 3.8). Finally, the morphology of each specimen varied according to the pH value. Specifically, at low pH the surface of the steel corrodes evenly and with continuous, harsh groves. When the pH is 4.5, the geometry of the metal is relatively even but less intense and constant. Lastly, at the value of 5.7, the pits were formed from the rainwater trace and had an arbitrary distribution [31]. (Figure 3.9)

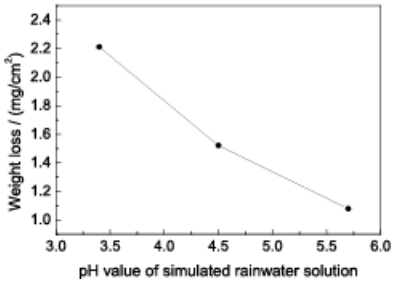

Figure 3. 8 Correlation of the Ph value of rainwater and the weight loss of the steel

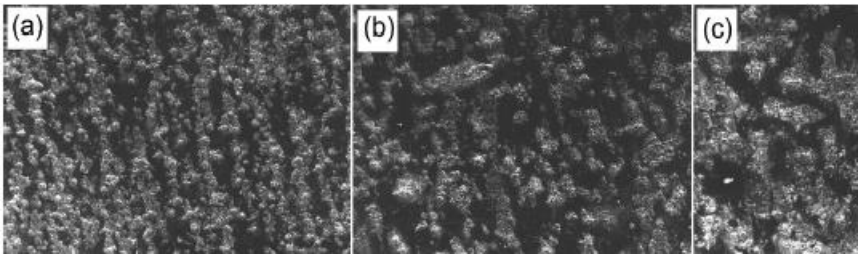

Figure 3. 9 Morphology of the A3 carbon steel at (a)3.9, (b)4.5, (5.7) pH values of the rainwater

3.1.3 Relative Humidity and Duration of Maceration

The duration of maceration defines the amount of time when the critical relative humidity is surpassed. In particular, below that humidity level, water does not develop on the steel surface, electrolysis is prevented, and corrosion is mitigated. Relative humidity (Rh) is determined through the percentage of the pressure of the water in vapor phase, compared to the saturation pressure. Namely, the critical relative humidity for steel is between 50% and 70%. Concurrently, corrosion is enhanced by the presence of pollutants in the atmosphere, such as sulfur dioxide and chloride ions. Thus, the critical value of relative humidity can drop to 40%. Also, the variation of humidity and

temperature leads to wetting and drying cycles that alter the rust mechanisms due to water evaporation and the salt deposit remaining on the surface.

Generally, it is observed that the humidity in the marine atmosphere is almost always above the critical value. Thus, according to Davis et al, for atmospheres with relative humidity (Rh) between 60-100%, its correlation with the atmospheric corrosion rate (d^o) of the steel can be accurately calculated through the Equation:

$$d^o = 0.3765[Rh] - 21.943 \quad for \quad 0.6 \leq Rh \leq 1$$

This model appears to be relatively linear (Figure 3.10), but it does not apply to humidity values beneath 60% ($d^o(0.6) = 0$). Finally, the variable R^2 is necessary to represent the accuracy of this model ($0<R^2<1$) [28].

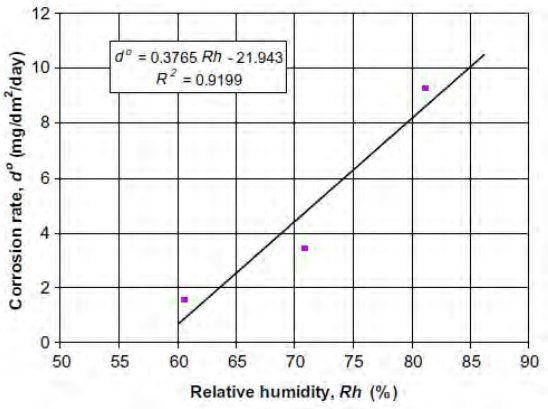

Figure 3. 10 Linear Correlation of corrosion rate and relative humidity

Furthermore, there is a straight correlation between humidity and air and surface temperature. The relative humidity is significant in temperatures within -5ºC and 15ºC. Above these percentages, the weather is warm and the water in the atmosphere is evaporated as well as the wet layer on the steel surface. Also, the corrosion current is reduced when the temperature is lower than -5 ºC, due to the formation of ice on the surface, and, simultaneously, chemical reactions can not occur because there is not enough kinetic energy of the molecules to provoke collisions. In the diagrams, it is visible that the highest corrosion rate of steel specimens is exceeded at 15ºC and 80% humidity [32]. (Figure 3.11)

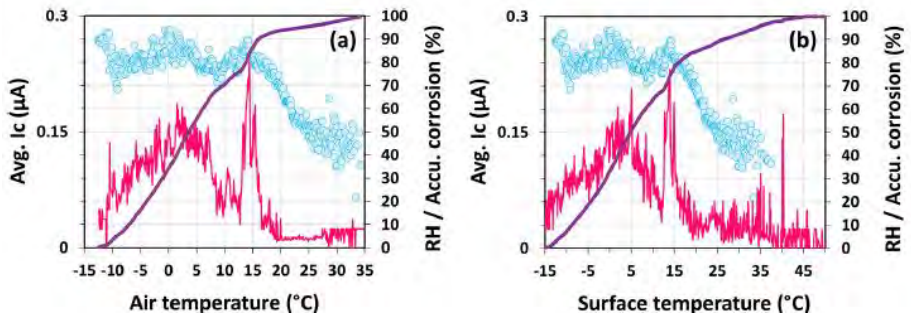

Figure 3. 11 Air and surface temperature and relative humidity (blue bubbles) as a function of the corrosion current (red line)

3.1.4 Saltwater Aerosol and Wind Speed

The deposition of sodium chloride can radically enhance the corrosion rate of the steel. Saltwater particles and droplets (salt aerosol) can be transferred by the wind alongside the ocean. However, for salt to have a vast influence on corrosion the particles should be above 10μm and moisture must be present on the metal surface. These conditions apply in the marine atmosphere, thus chloride ions are an important factor in atmospheric corrosion. Chloride ions (Cl^-) react initially with the Ferrum molecule and produce ferrous chloride ($FeCl_2$), which is soluble in water. Therefore, $FeCl_2$ transmutes the water at the surface into an electrolyte, with high acidity due to the formation of HCl ($FeCl_2 + H_2O \rightarrow FeO + 2HCl$). Furthermore, the cathodic reaction is provoked ($2H^+ + 2e^- \rightarrow H_2$) which leads to the transfer of electrons and hence the acceleration of the steel corrosion [27].

A test was conducted at Kure Beach in North Carolina, to determine the corrosion rate as a function of chloride concentration. The test took place 800 feet away from the shore as well as 80 feet away, where the concentration of the chloride ions was significantly higher. The accuracy coefficient for this model was R^2=0.55 and the correlation between corrosion and salt deposition appears to be linear (Equation 5).

$$d^o = 0.184[Cl] + 69.062 \qquad (5)$$

However, in the diagram (Figure 3.12) the relatively small fitting coefficient R^2 can be observed, because the data do not accurately approach the fitting line.

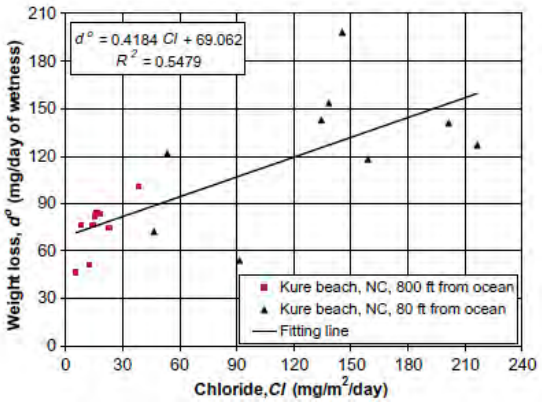

Figure 3. 12 Atmospheric corrosion rate as a function of the weight loss

Saltwater aerosol is created by breaking waves, and it is subjected to wind speed and impingement on the steel surface. Different wind speeds lead to different corrosion rates (Figure 3.13). Specifically, the larger values of average free corrosion currents (Ic), at a survey conducted on steel specimens, were noted at wind velocities between 5m/s and 17m/s, because of the transfer of particles and their impingement on the steel. Also, the waves break at a wind speed of 7m/s, which explains the increase in corrosion rate. When the wind surpasses 17m/s the current seems to drop, possibly due to the increase of the waves that wash away the remaining salt deposition.

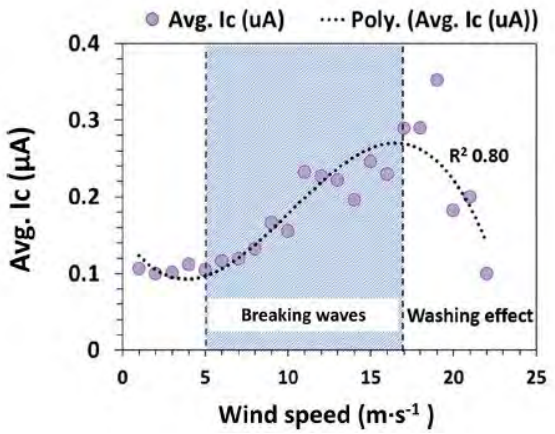

Figure 3. 13 Correlation between wind speed (m/s) and the average corrosion current

The synergy of the time of condensation, relative humidity, temperature, and time of wind velocities above 5m/s, contribute to atmospheric corrosion and they act collectively [28], [31], [32].

3.2 Flow Accelerated Corrosion, Erosion Corrosion and Cavitation

Flow Accelerated Corrosion (FAC) is one of the most crucial forms of corrosion that afflict carbon steel which is radically used in maritime engineering. As stated previously, a passive layer formation on the carbon steel surface is difficult due to its low content of chromium and nickel components. Thus, the constant motion of ocean water from underwater and wind currents as well as the movement of the vessel, leads to high corrosion rates and the destruction of the metal. Flow-accelerated corrosion and erosion-corrosion are provoked by the movement of the fluid relative to the steel surface, especially when the velocity of the vessel reaches above the critical value of 8-10m/s, where the sheer stresses from the fluid are increased. At lower speeds, the re-passivation phenomenon can occur when the external film is removed from friction, but above the critical values, it is not possible. Velocity, though, is not the only factor that generates FAC. The rust film produced in moving natural seawater plays a rather important role in the weight loss of the material. The formation of a thick rust layer in flowing ocean water operates as a protection for the steel surface and mitigates the flow-accelerated corrosion process.

Furthermore, erosion-corrosion can escalate this damaging process, due to the synergy of electrochemical reactions and mechanical wear of the metal. Viz, saltwater contains abrasive particles such as sand that impinge on the steel surface, reduce its thickness, facilitate mechanical fracture, and therefore, enhance the erosion mechanism.

3.2.1 Flow Accelerated Corrosion and Erosion Corrosion Experiment

An experiment was conducted on common marine carbon steel, EH 32, in both pure natural seawater, without the presence of abrasive particles, and in seawater with sand content, in order to study flow accelerated corrosion as well as erosion-corrosion. There was a variety of flow rates to determine the different rust film and damage.

The results for the FAC test (Figure 3.14) showed that above 3m/s flow rates, the corrosion process is increased through the duration of 12 hours. This phenomenon eventuates since the sheer stress from the fluid removes the passive layer from the steel surface and it can not be formed again due to the movement of the water. Nevertheless, when the water is moving at 1m/s, is almost stagnant and there is not enough oxygen transfer to generate the protective film, so the corrosive environment of the sea penetrates the steel, and the corrosion rate is high. As time passes, more oxygen

molecules are transported to the steel surface and the rust film is created which can protect the material from corrosion.

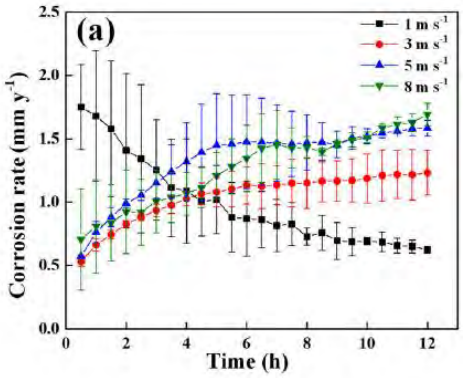

Figure 3. 14 Corrosion rate for different flow velocities over time

In Figure 3.15 the different morphologies and rust layers are presented as photos of the surface of the coupons (Figures 3.15a, c, e, g) and as images from the results of the scanning electron microscopy (SEM), (Figures 3.15b, d, f, h). The flow marks can be observed at each testing velocity (Figure 3.15a, c, e, g) as well as the rust coating, which is darker as the speed increases. At 1m/s the tip of the stream is formed at the center and the rust, which has a uniform distribution, has covered the steel at the downstream flow direction. At higher velocities, the rust layer is scattered with 'comet tails' morphology and it appears similar at flow rate speeds above 3m/s. Chemical analysis indicated that the corrosion products are comprised of magnetite and lepidocrocite, which protect the steel and they are not removed from the sheer forces of the flow stream. Thus, it is evident that erosion does not have a significant impact on natural seawater.

Moreover, the images of the SEM analysis present the appearance of the rusted surface. In Figure 3.15b, a portion of the outer rust coating, which has slid off the steel surface due to the loose and porous nature of the layer formed at 1 m s−1. The outermost layer of rust can be detected as spherical particles with distinguishable holes. The inner deposit has a geometry resembling glass. At greater velocities, the outer rust film is denser with rounder figuration, but the cracks can be visible. (Figure 3.15d, f, h)

When the corrosion products were removed, the areas underneath were corroded. Specifically, at 1m/s, a formation of small pits in the middle of the coupon was observed, which generated the flow accelerated corrosion. Eventually, these local pits were spread to "flow marks" (Figure 3.16a). When the flow velocity increased to 3 m/s,

the corrosion pattern would shift from "flow marks" to pits (Figure 3.16b). Furthermore, at enhanced flow speeds (5 and 8m/s), it is evident that the density of the pits increases (Figure 3.16c, d). Measurements determined that the depths of the pits ranged between 50 and 70 μm, at velocities between 3 and 8m/s, whilst the greatest value was observed at 8m/s, where few deep pits reached a maximum depth of 100 μm (Figure 3.16d). This phenomenon proves that higher seawater velocities result in larger corrosion damage.

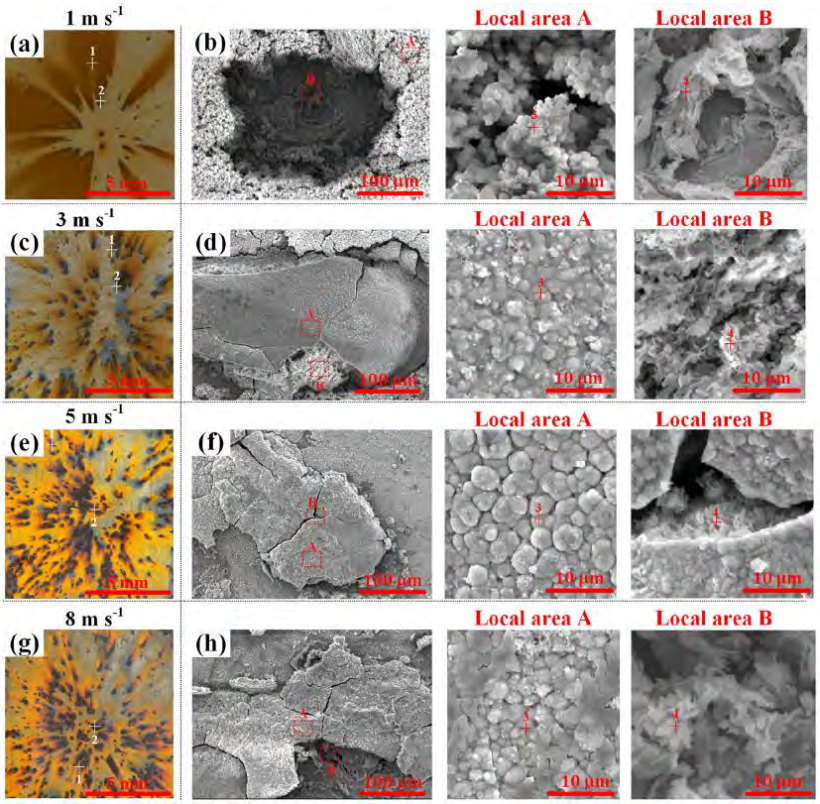

Figure 3. 15 (a, c, e, g) Photos of the morphology of the rust layer of the steel coupons at different velocities after the FAC mechanism, (b, d, f, h) SEM images of the outer and inner areas of the rust layer.

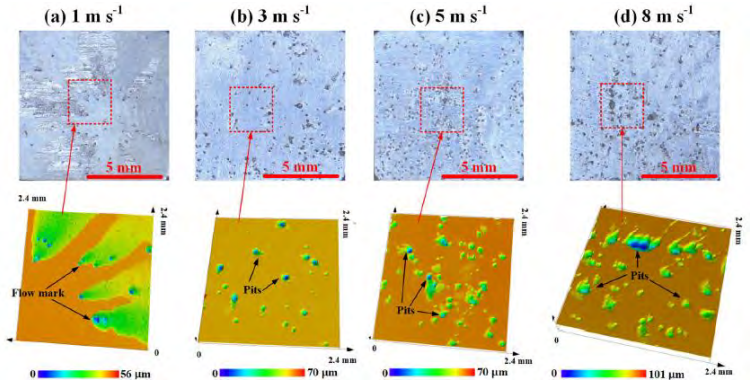

Figure 3. 16 The geometry of the corroded areas of the steel coupons after being tested for FAC at different flow velocities

At the erosion tests on EH 32 steel, pure erosion was enhanced by the impingement of sand particles. The pure erosion rate (W_{e0}) is dependent on the material constant (K), the abrasive particle's velocity (v), which is the same as the flow stream, and the material-specific velocity exponent (α), whose value fluctuates between 2 and 3 for metals. Finally, the accuracy coefficient used for this model was R^2=0.96.

$$\dot{W}_{e0} = Kv^{a}$$

The test results were plotted on the graph (Figure 3.17a). It is observed that at low velocities (1 and 3 m/s) the pure erosion rate is negligible, but it radically increases when the flow speed is accelerated from 5 to 8m/s.

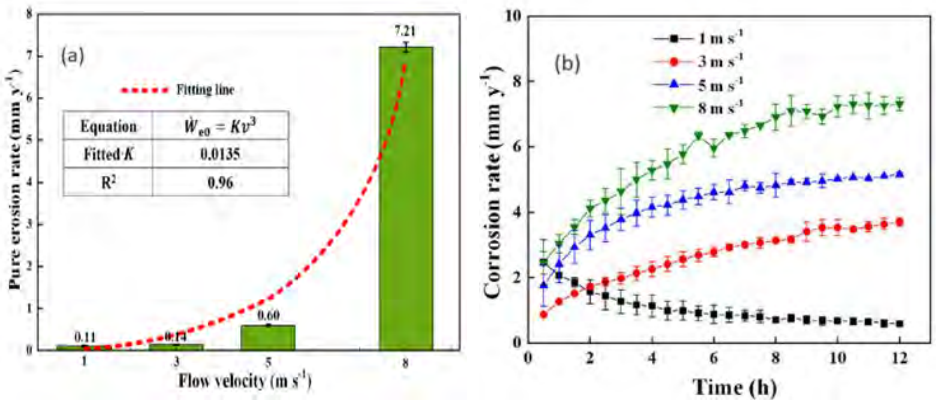

Figure 3. 17 (a) Pure erosion rate as a function of flow velocity, (b) Erosion-corrosion rate as a function of time.

The behavior of erosion-corrosion at a flow speed of 1m/s appears to be similar to the one of flow-accelerated corrosion since the rate decreases at the duration of 12h. Contrary to the sample which is drenched by the flow stream of 1m/s, all the other coupons, with higher flow velocities (3, 5, 8m/s) had a vast increase in the corrosion rate. At the velocity of 8m/s corrosion reaches the value of 7.31mm/year, concurrently, the variation of the rate is also intense since the slope of the curve seems to increase rapidly. (Figure 3.17b)

Images of the steel surface after the 12h experiment, indicate that the format of the flow marks is comparable to the FAC performance at 1 m/s, with a porous brown rust film (Figure 3.18a). At 3 m/s, several sporadic pits emerge on the steel surface and the flow marks regions shrink, and they contain the majority of the corrosion products (Figure 3.18c). When the flow velocity is accelerated to 5 m/s and 8 m/s, the erosion-corrosion

morphologies manifest as total pitting degradation (Figure 3.18e, g). Likewise, with the FAC procedure, the corrosion products formed on the outer surface of the samples are magnetite and lepidocrocite.

Furthermore, the SEM analysis defined the morphology of the rust layer and the pitting area. At 1m/s the outermost and inner regions of the rusted surface did not appear to have significant differences from the one after the FAC experiment (Figure 3.18d, f). However, at the other tested flow velocities, the main disparity is that the corrosion products are located only inside the pits and the flow marks, whereas the surrounding area is pure steel debris from the impingement of the sand particles. Interestingly, at the flow speed of 8m/s, in local area B, a small crevice is spotted between the pit ring and the debris (Figure 3.18h).

After the samples were cleansed from the corrosion products and the debris, the metal surfaces showed severe local corrosion, except the coupon which was impacted with 1m/s flow velocity. The flow marks presented in Figure 3.19a are similar to the ones in flow accelerated corrosion testing since the sand particles at 1m/s were unable to remove the corrosion products. The primary morphology transforms to a combination of small flow marks and pits with tails in the downstream direction as the flow velocity reaches 3 m/s. The pits located at the leading edge of the "flow mark" are substantially deeper than the average pit depth of the FAC process, reaching up to 100 μm (Figure 3.19b). At 5 m/s, the typical pit depth rises to 95−110 μm and the pits become more circular (Figure 3.19c). As the impingement velocity develops to 8 m/s, the quantity of the pits increases significantly (Figure 3.19d). Nonetheless, the average pit depth of 8 m/s is comparable to that of 5 m/s, indicating that the longitudinal expansion of the pits is almost unaffected by the rise in the kinetic energy of the abrasive particles.

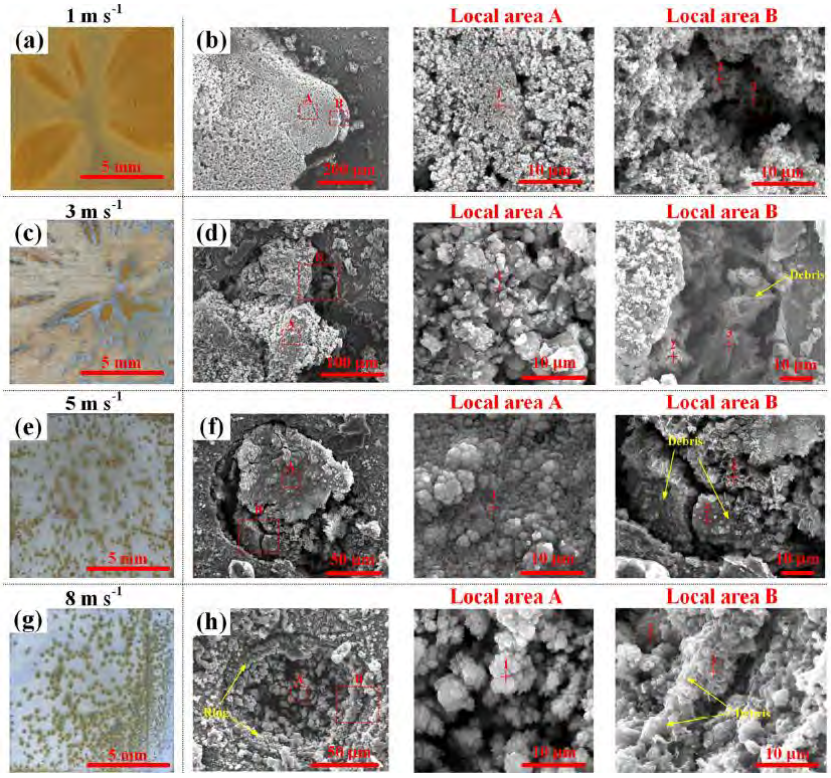

Figure 3. 18 (a, c, e, g) Photos of the morphology of the rust layer of the steel coupons at different velocities after erosion-corrosion mechanism, (b, d, f, h) SEM images of the outer and inner areas of the rust layer.

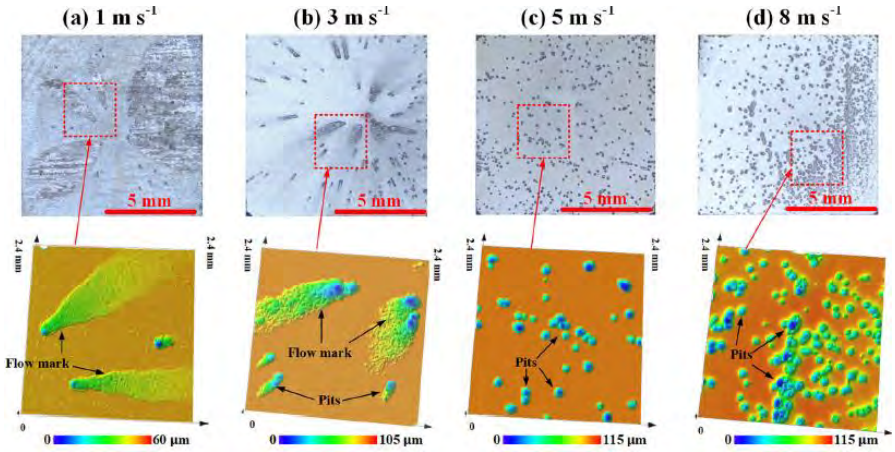

Figure 3. 19 Corroded surfaces of the coupons after the removal of the rust layer, at different flow velocities.

The conclusion of this survey was that Flow accelerated corrosion and erosion-corrosion of steel in natural saltwater, are influenced by numerous parameters, such as the rust film and the corrosion products, the flow and hydrodynamics, the electrochemical conditions, and finally the impact of particles contained in the fluid. Besides, the morphology of the metal surface during this procedure is variant, due to the formation of the rust layer and pits. This irregular geometry provokes turbulence

and accelerates the corrosion mechanism. Lastly, the transformation of the flow marks to pits indicated the progression of the FAC and erosion-corrosion process.

3.2.2 Cavitation

Finally, as was stated previously, a form of erosion-corrosion with a massive impact on marine structures is cavitation. It is more frequent in accelerated flows and turbulent flows due to the variation of pressure and velocity. Cavitation is a two-phase phenomenon, which occurs when the fluid pressure is reduced to a value of its vaporization (Pv) at the ambient temperature. Thus, the generation of vapor and steam bubbles is provoked as well as the production of voids and cavities. Cavities are observed to be either fixed or traveling, depending on their position. The fixed cavities have a smooth and glassy morphology, they are separated from the flow alongside the structure, and they are attached to the solid body. Contrastingly, traveling cavities move along the streamlines surrounding the material. (Figure 40)

When the bubbles enter a region where the pressure is increased, they collapse, which leads to the development of micro-jets and shock waves. The microjets form when the implosion occurs next to a solid boundary, and they are directed toward the solid surface with extremely high velocity. Consequently, there is a vast impingement on the metal surface and a significant increase in stresses. Therefore, the surface is severely abraded, especially in anodic areas, which results in the formation of stable pits, which provoke turbulent flow and intensify the damage. In addition, this mechanism allows traveling cavities to re-enter the fixed cavity and enhance the vapor phase. Hence, this two-phased phenomenon is enhanced, and the corrosion damage is continued. Furthermore, experimental studies have proven that cavities that implode onto a mild steel surface have caused an extreme local temperature to increase to the value of 400ºC. [40], [41]

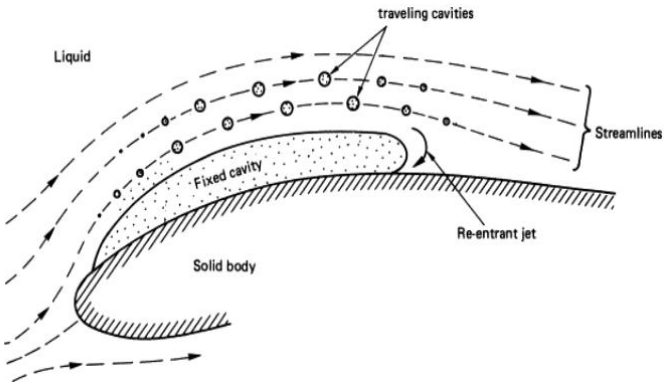

Figure 3. 20

For the determination of the existence of cavitation, the pressure and fluid velocity correlation is necessary. The Bernoulli equation proves that with the drop in the fluid's speed, there is an increase in static pressure (Ps), and therefore there is a higher risk of cavitation.

$$\frac{\rho}{2}v_A^2 + \rho g h_A + P_s = \frac{\rho}{2}v_2^2 + \rho g h_2 + P_2$$

The cavitation number can also be calculated through the following equation, which indicates that the higher the value (σ) is, the lower the probability is for cavitation to appear.

$$\sigma = \frac{Ps - Pv}{\frac{1}{2}\rho v_A^2}$$

It is observed that when the static pressure is equal to the vaporization pressure of seawater (Pv=175.7Kpa/m^2 for seawater at 15C^o), the existence of cavitation is initiated. Moreover, cavitation is dependent on the dynamic pressure ($q = \frac{1}{2}\rho v^2$), which is equivalent to the flow speed. It is comprehensible that the acceleration of the flow speed leads to the rise of the dynamic pressure and hence the increase of the probability of cavitation appearance. [41], [42]

Cavitation corrosion is present in turbines, ship propellers, rudders, hydraulic pumps, valves, pipes, and other areas with abrupt variations in static pressure. It is also prominent in regions with high vibrations, such as engine pistons and liners (Figure 3.20) [42], [1].

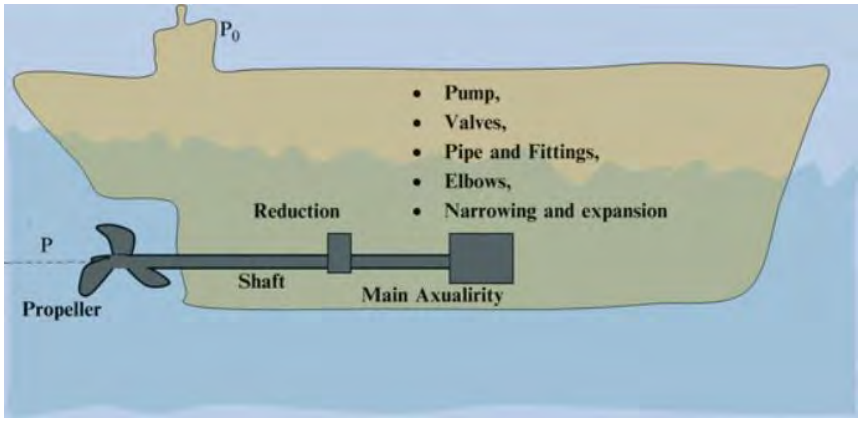

Figure 3. 21 Areas of the ship that are prone to cavitation

The propellers are one of the most crucial parts of the ship that are directly affected by cavitation and erosion corrosion, due to the impact with abrasive particles or buoyant objects. The propeller generates thrust by absorbing the torque or delivered horsepower, produced by the engine at specific revolutions, in order to move the ship through the water. Bernoulli's law states that as a hydrofoil, a region on the impeller's blade, passes through water, the pressure on the blade's face is positive, and on its backside is negative. The propeller's torque requirement and thrust generation are determined by how the pressures are resolved. At the negative pressure area, cavitation is initiated, and bubbles are formed.

Cavitation in propellers occurs in four main patterns, vortex cavitation or tip-hub, sheet cavitation, bubble cavitation, and cloud cavitation.

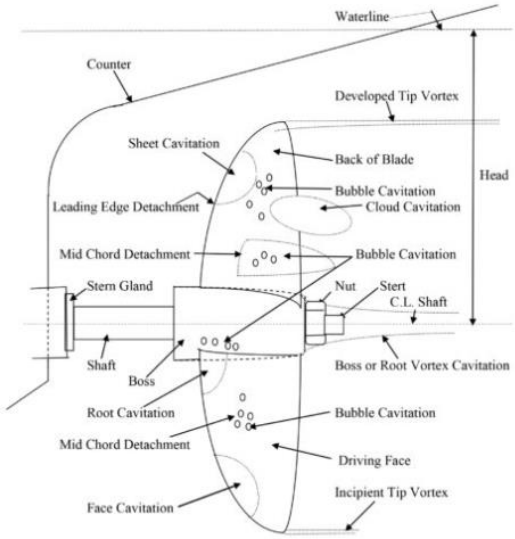

Figure 3. 22 Different forms of cavitation on the ship's propeller.

Sheet cavitation is evident as a stationary thin layer either, at the leading edge on the back of a propeller's blade, if the hydrofoil is operating at a positive incidence angle, or at the face of the blade if it is operating at a negative angle (Figure 42). Sheet cavitation develops due to high-pressure reduction and suction on the back of the blade, which occurs because of the intense flow velocity of seawater at this section. [43], [41], [42]

As the phenomenon evolves, breakage under stable sheet cavities might be developed. Particularly, a re-entrant jet that flows from the trailing edge to the front end of a sheet cavity causes it to collapse. As a result, the sheet cavity sheds near its leading edge and is hurled downstream as a cloud or mist of small bubbles and it is called cloud cavitation. (Figure 3.22) It is a highly unstable and dangerous form of damage since it provokes noise and oscillations to the flow which cause a vast degradation of the solid material. [45], [44].

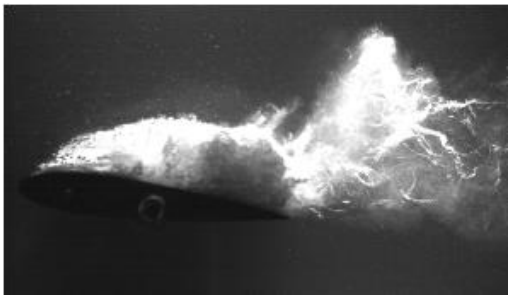

Figure 3. 23 Sheet and Cloud Cavitation on a Hydrofoil

Bubble cavitation is the formation of individual bubble cavities that expand over the blade surface and compress quickly, sometimes becoming rather large. They primarily appear in the middle area of the blade of the propeller (Figure 42). This type of cavitation is enhanced by the intensity of the curved geometry of the blade section due to the fluctuation of the velocity and pressure.

Lastly, vortex types of cavitation are evident at the leading edge of the propeller blade, the tip of the blade, and the boss or hub of the propeller. They are mainly provoked due to the low pressure in the areas where the vortices shed. The primary form that is the first to appear is tip or hub vortex cavitation which is developed due to the high water flow angle relative to the propeller blade. It deforms the edge of the blade and deteriorates the dynamic performance of the propeller, affecting the thrust, the load distribution, and producing oscillation. Sometimes, vortices tend to collapse on the tip

of the blade, causing serious erosion damage and pitting (Figure 3.23). Also, vortex cavitation generates noise which was often used to detect the location of the ships. [42], [43], [44]

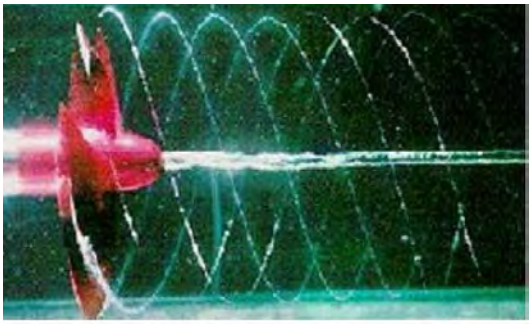

Figure 3. 24 Tip vortex cavitation on a propeller.

The appearance of cavitation can also be determined by the number of the propeller's revolutions (N). At low revolutions, tip vortex cavitation can be present, but as the revolutions increase as well as the linear velocity, sheet cavitation is generated. Finally, when the number is significantly high, there is an extended form of sheet cavitation with the consequent formation of bubble cavitation. (Figure 3.23) [40]

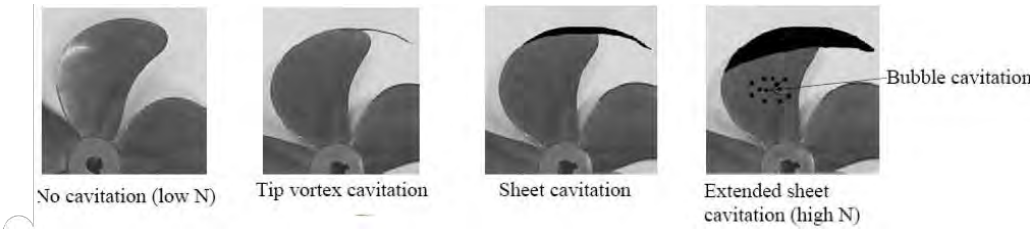

Figure 3. 25 The formation of cavitation with the rise of the propeller's revolutions (N)

Cavitation damage can be distinguished at early stages. The first indication of the problem is the initiation of the designated orange peel effect, in which the surface experiences ductile deformation and appears similar to the orange morphology. Damage may either stop or continue after that initial phase, depending on the intensity of the attack. Microhardness testing on both torn and intact blades reveals that the material in the layers directly beneath the surface hardens and becomes brittle when subjected to cavitation assault. The tests indicate that, in the case of undamaged blades, there is a very slight change in hardness that occurs just below the surface and is most likely the result of the finishing and manufacturing procedures. Thus, the marine

surveyor should anticipate that the material would fail under cavitation attack and that the failure will have a significant amount of brittleness.

3.3 Galvanic Corrosion

Galvanic Corrosion or biometallic corrosion is a type of corrosion that occurs through an electrochemical process happening when two metals are in contact. Galvanic corrosion appears when two different metals are inside a conductive mean and therefore electrically connected with each other. These two different materials work as a cathode–anode pair and one of them is corroded (the anode) while the other is protected (the cathode). This type of corrosion appears often in marine structures and in seawater environments where seawater acts as the conductive solution where galvanic corrosion can begin. It is common to detect galvanic corrosion in ship weldings where carbon steel is welded using a different type of weldment. Moreover, aluminum devices that come in contact with carbon steel on ships or offshore structures tend to corrode due to this electrochemical process [52].

Galvanic corrosion as stated before can be detected in lots of ways on a vessel when different materials are in contact and seawater is present. Using steel or copper fasteners on an aluminum hull, mixing different types of metallic paint on the same ship, or placing an aluminum mooring fitting (or other equipment) on a carbon steel vessel are some of the reasons galvanic corrosion appears on vessels and can be catastrophic for the structure [53].

The first technical report, submitted in 1763, that galvanic corrosion appeared to have provoked problems to a vessel concerned the English frigate “Alarm”. This frigate had been reinforced with copper so that the wood on the vessel was not polluted by shipworms. The copper plates attached to the ship were fixed with iron nails and after two years of the ship sailing, during the maintenance period, it was discovered that most of the copper placed had been lost. Further investigation showed that the iron nails used were corroded and caused the detachment of the copper plates which led to the conclusion that direct contact between copper and iron should be avoided in seawater environments [54]. In Figure 3.24 the remains of the iron bolts used in the frigate are shown with corrosion damage being obvious.

Figure 3. 26 Remains of iron bolts used in the 1763 frigate incident

The main factor affecting galvanic corrosion is the temperature. A study on galvanic corrosion was conducted at Harbin Engineering University in China, where the high-strength steel 921A with Cu-Ni alloys was tested for galvanic corrosion. The experiment was conducted using plates as samples submerged in stagnant seawater with different temperatures. Galvanic corrosion currents were measured using a zero-resistance ammeter (ZRA). A ZRA device measures the current flowing through it without adding resistance to the electric circuit.

The experiment resulted in the equation below indicating the corrosion rate V_t is a function of the sample dimensions.

$$V_t = \frac{8.76 \cdot 10^7 \cdot (M - M_1)}{S \cdot T \cdot D}$$

where S is the total surface of the corroded sample, T is the time of immersion of the sample, and D is the density. Furthermore, M is the mass of the sample before the corrosion, and M_1 the mass of the sample after the corrosion.

In Figure 3.25 the electrical current flowing through the 921A high-strength steel is depicted for seawater in different temperatures.

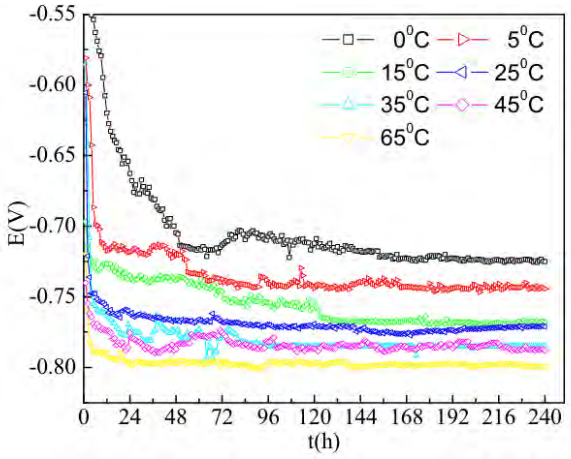

Figure 3. 27 Electrical Current vs Time for varying seawater temperatures Electrical Current vs Time for varying seawater temperatures

It is clearly visible that the higher the temperature of the solution that the sample was submerged the bigger the rate of electrical current passing through the sample [55].

It is important to note that in the particular experiment where high-strength steel and Cu-Ni alloys were tested the 921A high-strength steel acted as the anode and the Cu-Ni alloy acted as the cathode. As stated before the anode component of the galvanic reaction is the one that gets damaged while the cathode component is the one protected [56]. It is prevalent for the steel component to act as the anode on the galvanic reaction because of its content in Mn.

A chart showing the voltage range of alloys in flowing seawater is presented in Figure 3.26. This chart helps determine the anode and cathode of a pair of metals met underwater.

Table 1
GALVANIC SERIES
In Flowing Seawater

Alloy		*Voltage Range of Alloy vs. Reference Electrode**
Magnesium	**Anodic or Active End**	-1.60 to -1.63
Zinc		-0.98 to -1.03
Aluminum Alloys		-0.70 to -0.90
Cadmium		-0.70 to -0.76
Cast Irons		-0.60 to -0.72
Steel		-0.60 to -0.70
Aluminum Bronze		-0.30 to -0.40
Red Brass, Yellow Brass, Naval Brass		-0.30 to -0.40
Copper		-0.28 to -0.36
Lead-Tin Solder (50/50)		-0.26 to -0.35
Admiralty Brass		-0.25 to -0.34
Manganese Bronze		-0.25 to -0.33
Silicon Bronze		-0.24 to -0.27
400 Series Stainless Steels**		-0.20 to -0.35
90-10 Copper-Nickel		-0.21 to -0.28
Lead		-0.19 to -0.25
70-30 Copper-Nickel		-0.13 to -0.22
17-4 PH Stainless Steel †		-0.10 to -0.20
Silver		-0.09 to -0.14
Monel		-0.04 to -0.14
300 Series Stainless Steels ** †		-0.00 to -0.15
Titanium and Titanium Alloys †		+0.06 to -0.05
Inconel 625 †		+0.10 to -0.04
Hastelloy C-276 †		+0.10 to -0.04
Platinum †	**Cathodic or Noble End**	+0.25 to +0.18
Graphite		+0.30 to +0.20

* These numbers refer to a Saturated Calomel Electrode.
** In low-velocity or poorly aerated water, or inside crevices, these alloys may start to corrode and exhibit potentials near -0.5 V.
† When covered with slime films of marine bacteria, these alloys may exhibit potentials from +0.3 to +0.4 V.

Figure 3. 28 Galvanic Chart of Alloys

Despite temperature being a critical factor in galvanic corrosion, relative surface area, between the anode and the cathode, is an important factor in galvanic corrosion propagation. A common example showing the importance of the relative surface area is the case where the cathode component has a large surface area when the anode component has very small surface area. This case produces very large currents making the anode component corrode quickly.

Relative surface area is a common reason why galvanic corrosion appears at high rates around fasteners. In Figure 3.27(A) steel bolts are used to secure the stainless steel supports of a bridge. In this example, the steel bolts act as the anode component of the pair while the stainless steel supports act as the cathode component. The relatively small surface area of the steel bolts results in a very strong galvanic couple causing a high rate of galvanic corrosion. On the other hand, in Figure 3.27(B) stainless steel bolts

have been used to secure a carbon steel plate. In this incident, the cathode component of the pair is the stainless steel fastener while the anode component is the steel plate. Obviously, the surface area of the cathode is relatively insignificant, causing slow galvanic corrosion on the structure [57].

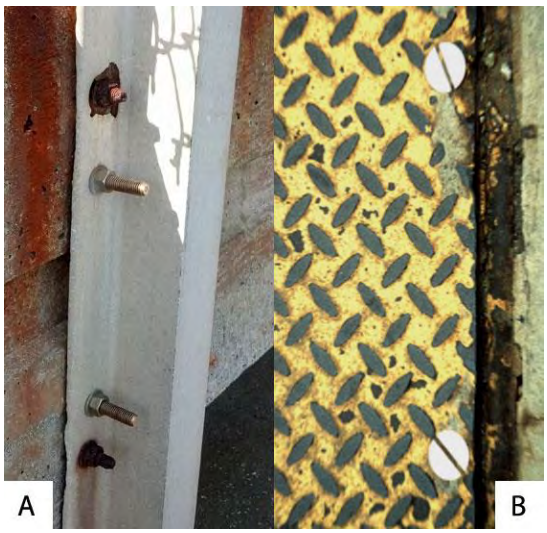

Figure 3. 29 Relative Surface Area effect on galvanic corrosion

The primary ship components affected by galvanic corrosion are the hull of the ship where usually different metal components attach like aluminum or bronze. Moreover, the Hull is constantly in touch with seawater (the conductive mean). Another typical area where galvanic corrosion appears is on the ship propellers which are typically made of bronze and come in contact with steel shafts. Furthermore, fasteners and fittings which were discussed before are common galvanic corrosion instances because they are used for the bonding of different materials, causing galvanic reactions. Last but not least, the paint used in ships causes big problems with galvanic corrosion and is one of the main maintenance concerns for vessels.

Figure 3. 30 (a) Galvanic corrosion on ship propeller, (b) Galvanic corrosion caused by metallic paint

To sum up, galvanic corrosion is a big failure factor that should be taken into consideration by marine engineers when designing marine structures or health monitoring of already built structures [58]. Figure 3.29 is one common example of galvanic corrosion of a bronze intake strainer on a steel boat that has been destroyed from galvanic corrosion.

Figure 3. 31 Bronze intake strainer destroyed from galvanic corrosion.

Chapter 4: Prevention Methods of Corrosion:

Corrosion protection in ships is vital to maintain safety, durability, and efficiency. In order to avoid the deterioration of the steel structure, it is necessary to apply the appropriate protection methods both during the design phase and during the official operation of the ship, in addition to the maintenance carried out as part of the regular inspection. These techniques can be classified into four groups: material selection during the design process, cathodic protection (mostly employing sacrificial anodes), protective coatings, and regular inspections.

4.1 Design Process

Corrosion prevention is strongly dependent on the design. For the selection of the final design it is necessary to take into account the following factors that greatly influence the effect of corrosion:

- The material selection
- The environment
- The construction limitations and the contact with other metallic surfaces

Specifically, material selection should be in compliance with international standards, such as ISO regulations. The steel used in the marine industry is usually low-cost and has medium mechanical strength. The selection is correlated with the environment that the area is exposed to.

For example, deck fittings are mostly made from stainless steel which contains chromium. Hence the material acquires anticorrosion quality because chromium reacts with the oxygen of the atmosphere and forms a protective layer which makes stainless steel resistant to corrosion and rust.

There are various elements that are used to enhance the properties of steel and contribute to the increase of corrosion resistance, such as nickel and molybdenum, nickel, and especially copper. When these metals react with oxygen, they develop a passive film that protects the steel. Copper alloys are regularly used in acidic environments with a high concentration of chromium. For alkaline conditions, stainless steel is preferable. [50], [52], [60]

In addition, very important is the correct preparation of the steel surface by using adequate machining techniques. Sharp edges should be rounded at a minimum radius of 2mm, rough areas should be smoothened and welds must be grounded. The procedures above are radical for the eradication of irregularities on the surface and they secure the coating application and prevent damage from flowing fluids and other corrosive mechanisms.

4.2 Cathodic Protection

Cathodic protection is one of the most effective ways to fight corrosion, is widely used in shipbuilding, and can confine almost all types of corrosion. It is an electrochemical method used to prevent corrosion of the metal structure through the generation of a continuous cathodic current.

Specifically, cathodic protection undermines the electrochemical reaction that occurs when the metal is exposed to a corrosive environment where the seawater acts as the electrolyte. During the electrochemical reaction, a negatively charged electrode known as the anode releases electrons and oxidizes, driving electrons away from the positively charged electrode known as the cathode. Thus, the steel structure, which needs to be protected, is transformed into a cathode and the surface becomes a non-corroding and protected electrochemical cell.

Two forms of cathodic protection processes are used in maritime, galvanizing, and impressed current.

Sacrificial anodes, used in galvanic cathodic suppression systems, are composed of a metal that is more reactive than the ship's hull, whilst the impressed current method in order to generate the electric current, an external source of power is used.

4.2.1 Cathodic Protection through Sacrificial Anodes

In the current method, more electropositive metals than the hull are fitted on the outer region of the ship. The most regular metals used as anodes are zinc, magnesium, and aluminum, which are more anodic than the hull’s steel. Thus, these metals are easier to corrode since the steel is converted into a cathode.

This thesis mentions sacrificial anodes, which work on the electrolysis principle. In electrolysis, when an anode and a metal come into contact with an electrolytic solution,

the anode electrons deposit over the metal, transforming it into a cathode. This simple transfer of electrons occurs regularly in ships due to the existence of seawater as an electrolyte (Figure 4.1). Using artificial anodes instead of the steel plates used in ships engineers direct the electrolysis in a specific anode-cathode pair that obviously protects the vessel.

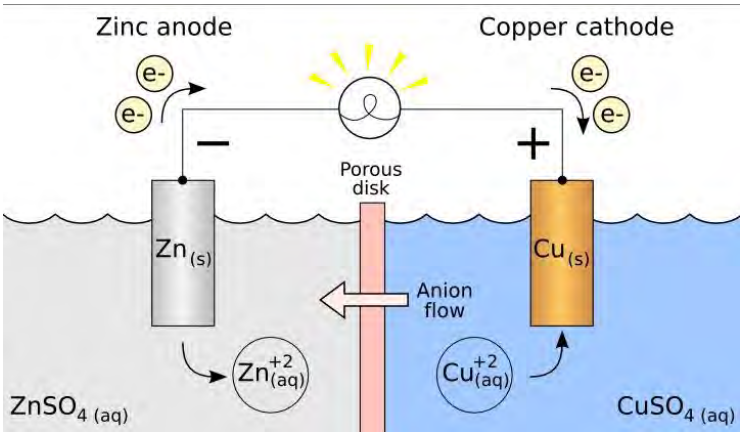

Figure 4. 1 Electrolysis

Sacrificial anodes are normally fastened to the ship's hull with bolts or welds. The anodes are positioned on the hull at key points, like the waterline, the vicinity of the propeller, and the bilge, where corrosion is most prone to happen. (Figure 4.2)

Figure 4. 2 Bronze intake strainer destroyed from galvanic corrosion.

These anodes only need to be replaced if they are completely worn out. Typically, these anodes are replaced every 2 to 3 years during dry docking. One of the key benefits of using this method is the minimal maintenance required. Despite the infrequent maintenance, the cathodic protection provided by sacrificial anodes can be easily installed and removed from the vessel using simple equipment such as welds, bolts, and brackets. Additionally, no external power source is necessary for this method to be effective. [51], [52]

Figure 4. 3 Large Vessel during maintenance of sacrificial anodes

4.2.2 Cathodic protection using externally imposed current (ICCP)

Cathode protection using externally imposed current is similar to the sacrificial anodes method with the difference that the electrolytic reaction is forced to happen with external currents. A system, which consists of 5 components, is constructed in order to implement the ICCP method. These components are:

1. The power source
2. The anode
3. The electrodes
4. The electrolytic environment
5. The structure protected

The cathodic protection system's algorithm commences with the power source generating and disseminating currents through the anode into the protected structure. These currents are negatively polarized to facilitate a voltage drop. Continuous current

flow from the power source is essential throughout the entire electrolytic reaction process to maintain the stability of forced and natural currents. The efficacy of the ICCP system is contingent upon the current density, which denotes the amount of current per unit area of the metal surface.

An array of materials can serve as anodes in the ICCP system, including cast iron, graphite, mixed metal oxide, and platinum protection using externally imposed current is considered better, because it offers a significantly longer life. This is because the anode is provided by an unlimited source of energy. To maintain the quality of the system, frequent maintenance is required [59].

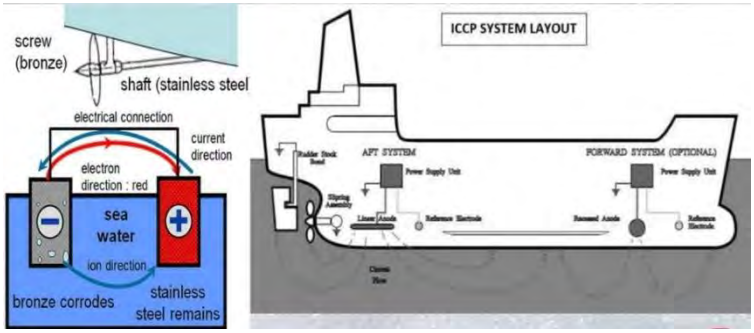

Figure 4. 4 ICCP explanation

4.2.3 Corrosion protection using paint

Lastly, the following prevention method, is the creation of a protective membrane in the hull which acts as a barrier, stopping the interaction of the environment and the construction. Before applying the paint, our construction must be properly treated (cleaning and smoothing the surface).

The colors consist mainly of:

- The carrier: It is the basic component of colors. Synthetic polymers are the basis for creating the protective film that adheres to the construction. The synthetic polymers of which it is composed are vinyl resins, chlorinated polymer resins, Tar, etc.
- Solvents and diluents: the main reason for their existence in paints is to facilitate their application. They facilitate the formation of the protective film.

Essentially, they modify the rheological characteristics of the colors in order to make them more uniform on the surface. When using them, special care is required as they are flammable materials. The risk is noticeably less once the paint dries. The most widely used are aromatic hydrocarbons, ketones, water, etc.

- Pigments and additives: pigments are organic in nature, while additives are natural minerals that have been processed. Pigments are divided into two categories, active and inactive. Their main difference lies in that active ones interrupt the anode process, while inactive ones reduce permeability and improve adhesion properties. Additives stabilize the thickness of the membrane and shape its properties. The best-known inert additives are the titanium, iron, and zinc oxides. [59], [60]

Chapter 5: Sensitivity Analysis of Corrosion with SOLIDWORKS Simulation:

The purpose of this analysis is to assess the extent of corrosion damage on the upper deck of a bulk carrier and the reinforcement plating that underpins it. This will be accomplished by comparing the stress levels before and after corrosion has occurred.

5.1. Explanation of the structural design of the deck

The motor vessel that is used as a reference is a bulk carrier built in 2012. Its overall length is above 250 meters, and its width is approximately 30 meters. For the purpose of the study, the 3D design is based on the aft area of the ship, where the mooring fittings were installed. Particularly, the relevant illustrated region ranges from frame -7 to frame 5 and abstains from the center line (CL) 7026mm starboard and -2739 port side. (Figure 5.1)

The software used for the 3D modeling is SolidWorks. The depiction of the upper deck, the correct placement, and construction of the underdeck stiffeners as well as the location of the mooring equipment depend on the structural designs of the ship and the 2D drawing of the fittings which was made in AutoCAD. (Figure 5.2)

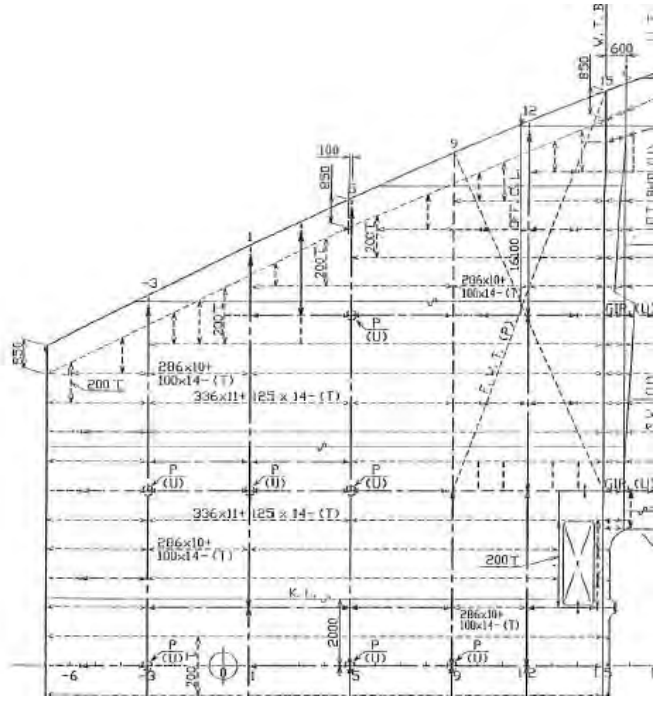

Figure 5. 1 Original 2D structural drawing

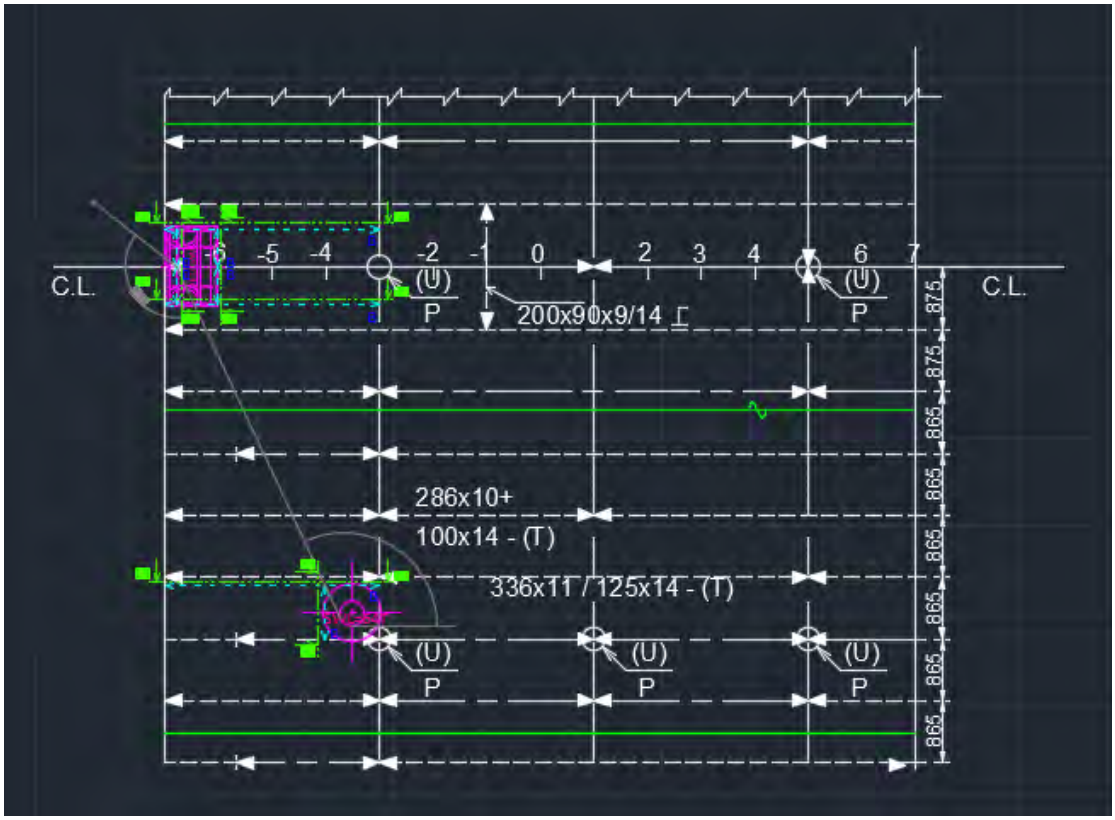

Figure 5. 2 Structural Design of the upper deck with the mooring fittings (AutoCAD)

In order to design the following part, the chosen dimensions and stiffeners are indicated in Table 3.

Table 3 Principal Dimensions

Table 3	
Frame Spacing	750mm
Deck plating thickness	13mm
Transverse Girders (Every 4 Frames)	(T) 800x12 / 200x14
Longitudinal Stiffeners	(L) 200x90x 9/14 (Except as shown)
Pillars	Ø318x12

The terminology used above (Table 3) is shown in Figure 5.4, where a typical underdeck structure is depicted.

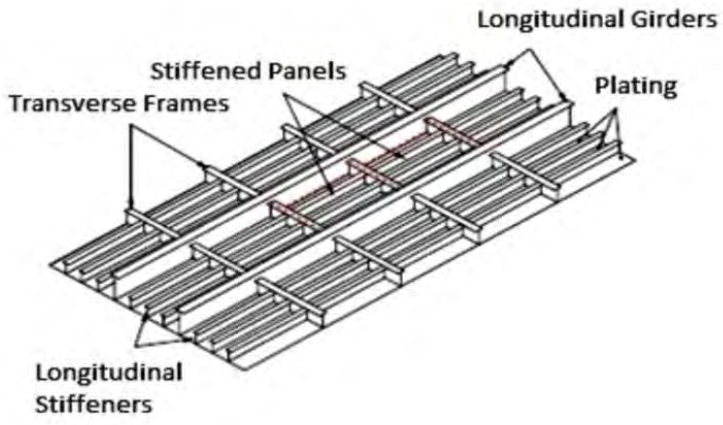

Figure 5. 3 Typical underdeck construction

The deck was reinforced with new strengthening plating to support the installation of mooring fittings. This addition is essential for safe operation because the areas where this equipment is located overcome intense loads not only due to the extra weight but also because of the rope tension which can reach 2000-7000kN [46].

The new stiffeners are presented in Figure 5.5 and are listed in Tables 4 and 5.

Table 4 Added Structure Under Mooring Chock

Table 4		
ADDED STRUCTURE UNDER MOORING CHOCK		
Number	Type	Quantity
(1)	FB 450x18	2
(2)	FB 450x18	2
(3)	FL 150x18	4
(4)	(T) 450x18/ 150x18	2
(5)	FB 300X20	2
(6)	BRK 350X18	2
(7)	BRK 250X18	4

Table 5 Added Structure Under Roller Capstan.

Table 5		
ADDED STRUCTURE UNDER ROLLER CAPSTAN		
Number	Type	Quantity
(1)	(T) 450x18 / 150x18	2
(2)	(T) 450x18/ 150x18	2
(3)	FB 300X20	2
(4)	BRK 350X18	2
(5)	BRK 250X18	4

Where:

- FB: Flat Bar
- FL: Flange
- BRK: Bracket

The 3D design for the examined part of the vessel is shown in Figures 5.4, 5.5, and 5.6. This 3D model is used for the simulation process which is presented in the following section.

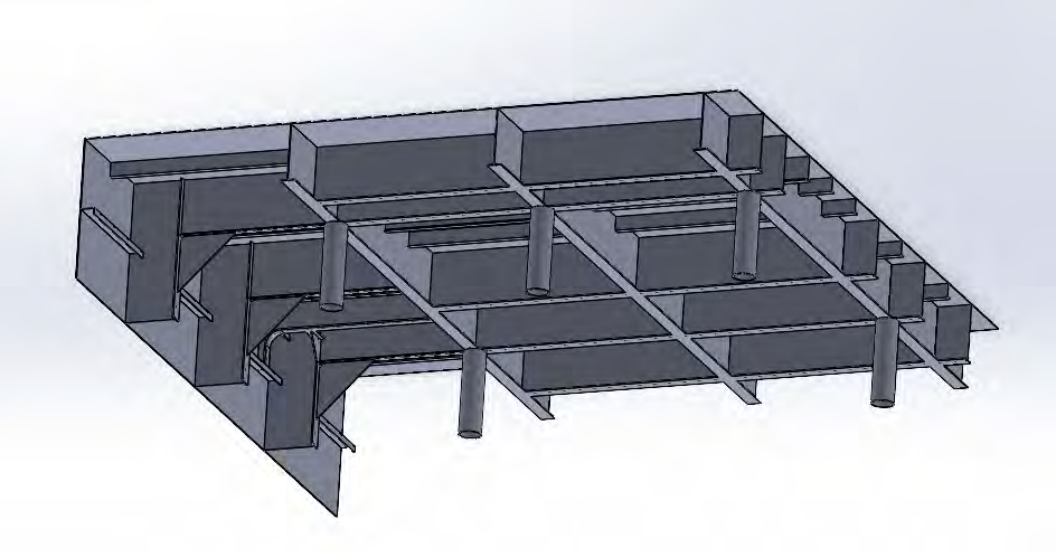

Figure 5. 4 SOLIDWORKS 3D model design Isometric view.

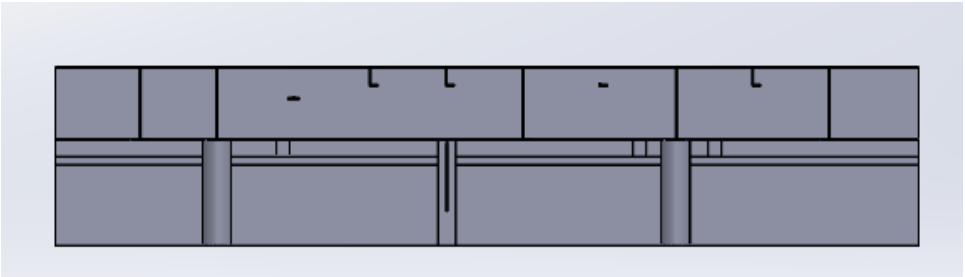

Figure 5. 5 SOLIDWORKS 3D model design, front view

Figure 5. 6 SOLIDWORKS 3D model design, Bottom view

Lastly, in order to place the deck mounted, closed mooring chock, and the wrapping roller with pedestal, split lines were created. These were used to indicate the fittings' location and apply the distributed loads for the FEA simulation.

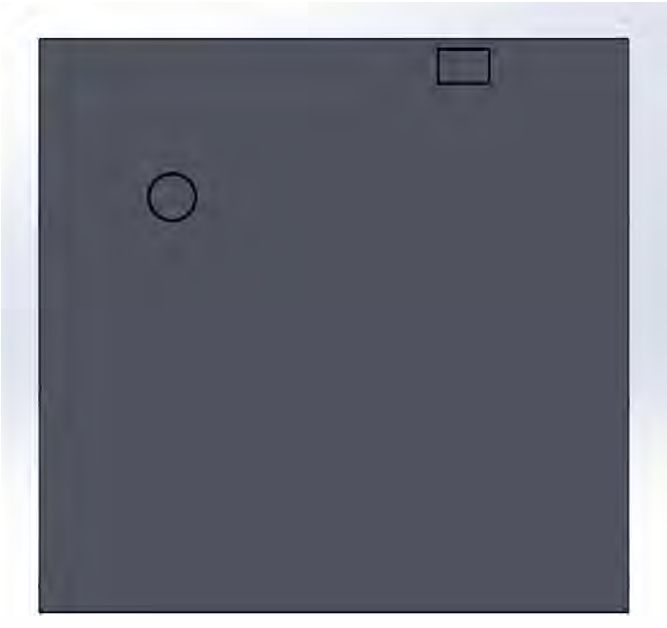

Figure 5. 7 SOLIDWORKS 3D model design, indicating split lines location

5.2 Simulation Process.

The aim of this simulation analysis is to observe how the loads applied on the mooring fittings can transfer to the ship's main structure and how these forces can generate stresses and displacement which can severely affect the ship's structural integrity.

The mooring equipment that was installed on the deck was approved and standardized by the classification society.

Specifically, the stand roller used for the mooring process is constructed following ISO 17736 standards. Its height is 1000mm and the diameter of the steel roller is 350mm. Depending on the table in Figure 5.8, its weight is 358 kg, and the safe working load is a maximum of 106 T for the operation of 90 degrees (Figure 5.8). The fitted roller is a capstan roller with a mechanism that wraps the rope using a rotating motion.

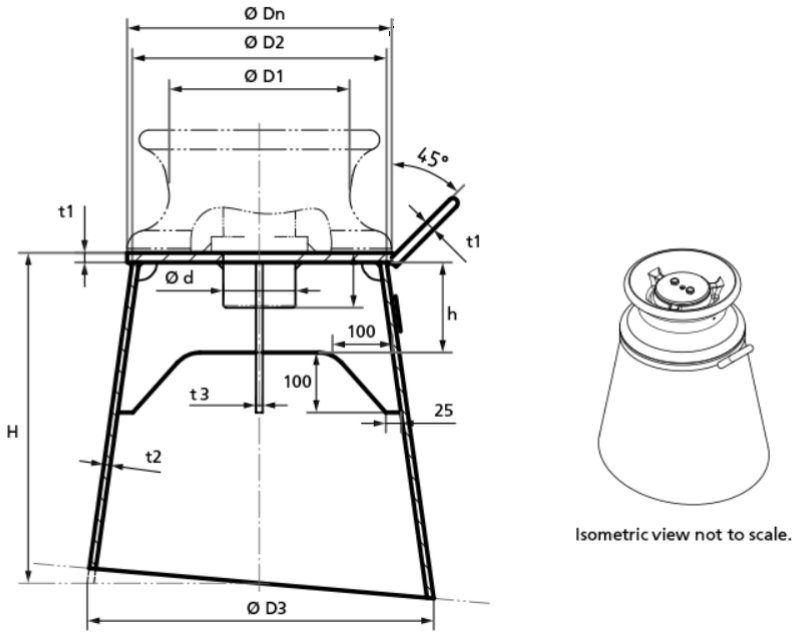

Nominal Size	Dimensions (mm)							SWL				Weight		
Dn			d					θ=90°		θ=0°		H=500	H=1000	H=1500
(mm)	D1	D2	Type A&B	Type C	h	t1	t2	(kN)	(t)	(kN)	(t)	(kg)		
150	220	230	71.5	81.5	200	16	10	265	27	186	19	55	115	198
200	288	300	93.5	102.5	200	20	12	441	45	314	32	86	169	278
250	357	370	113.5	119.5	200	22	12.5	579	59	412	42	113	210	335
300	417	430	128.5	130.5	225	24	13	726	74	510	52	145	256	395
350	472	490	145.5	152.5	225	26	17	1040	106	736	75	201	358	552
400	540	560	154.5	164.5	250	28	18	1246	127	883	90	255	436	657
450	600	620	167.5	179.5	250	30	20	1599	163	1128	115	314	530	791
500	655	680	178.5	195.5	250	32	22	1942	198	1373	140	383	636	938

Figure 5. 8 Pedestal Roller Fairlead ISO 13776 A350 [47]

The closed chock added to the vessel is manufactured in compliance with ISO 13729 standards and is deck-mounted type A. A ship that uses wire ropes is typically fitted with this form of mooring chock. Its nominal size is determined by the parameters (L*H*D) which are indicated in Figure 5.6. Particularly, in the model the dimensions are L=500, H=250, D=525 A [mm].

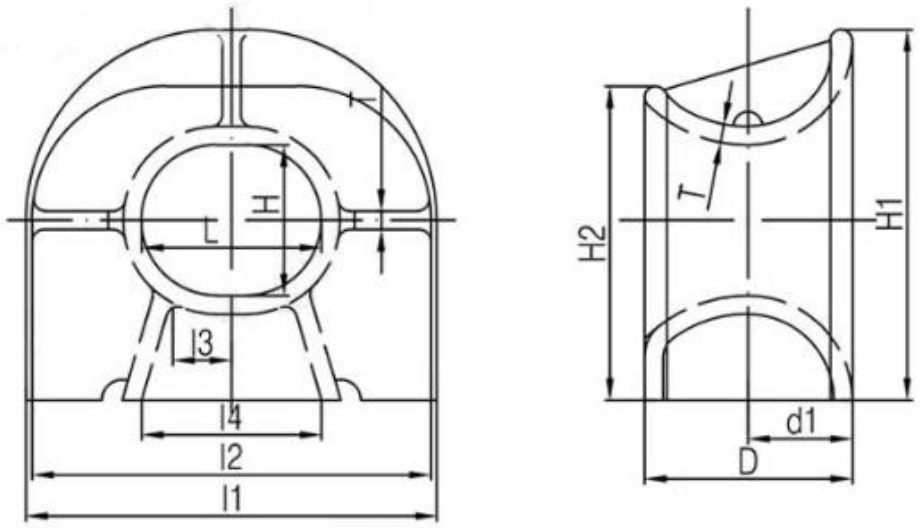

ISO13729 Deck Mounted Closed Chock (Type A)									
Nominal Size L*H*D (mm)	SWL (kN)	Dimensions(mm)						Weight (kg)	Wire Rope Dia. (mm)
		l1	l2	l3	l4	H1	H2		
250*200*214	226	488	453	76	265	427	368	73	18
300*250*286	422	614	565	89	330	551	481	142	24
350*250*333	549	716	660	114	403	601	525	22	28
400*250*381	687	820	754	139	475	652	553	310	32
450*250*381	706	870	804	164	524	652	553	322	32
500*250*381	765	920	854	189	574	553	553	337	32
400*250*428	883	870	796	139	500	609	609	434	36
450*250*428	912	920	846	164	550	609	609	452	36
500*250*428	932	970	896	189	600	609	609	472	36
500*400*428	893	970	896	176	600	759	759	528	36
500*250*525A	1148	1068	1000	190	652	675	675	657	44
500*400*525A	1158	1068	1000	193	652	825	825	724	44
500*250*525B	1413	1074	1000	176	652	680	680	753	44
500*400*525B	1383	1074	1000	179	652	830	830	825	44

Figure 5. 9 Closed Chock ISO 13729

For the FEA simulation study setup, fixtures and loads were applied, and finally, the mesh was modified to fit the geometry of the structure.

5.2.1 Fixtures

Three main fixtures were applied for the simulation: fixed geometry, symmetry fixture, and roller/slider fixture.

1. Fixed geometry

In SOLIDWORKS Finite Elements Analysis, fixed geometry is applied to the edges or faces of bodies and components so as to restrict their movement and all the degrees of freedom. In particular, this fixture prohibits the movement of solid bodies on the three axes (x, y, z) and the movement of beam elements on the rotating translational degrees of freedom too. [48]

Fixed geometry in this experiment is applied at the faces of the underdeck stiffeners and pillars because the geometry of the structures continues below the designed area. Therefore, the model has zero degrees of freedom and should not be able to move in any direction. (Figure 5.10)

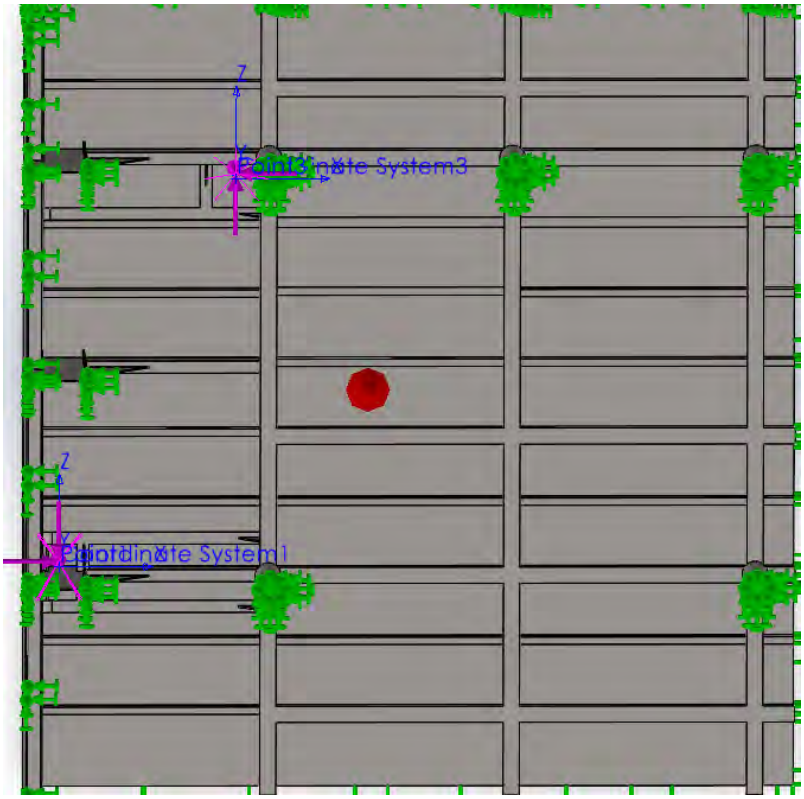

Figure 5. 10 Fixed Geometry at the under-deck construction.

2. Symmetry Fixture

Generally, symmetry can be used in SOLIDWORKS to model a section of the part rather than the entire construction. Hence, the results for the un-modeled problem are driven by the simulated part. It can be only used in planar faces. Furthermore, it prevents the concentration of stresses at this region due to the avoidance of torque development, and also to the existence of embedding, which in this case does not exist in this area. [48]

Thus, for this study, a symmetry fixture is applied on the left side of the part since the construction of the vessel is symmetrical, namely the port side is similar to the starboard side. (Figure 5.11)

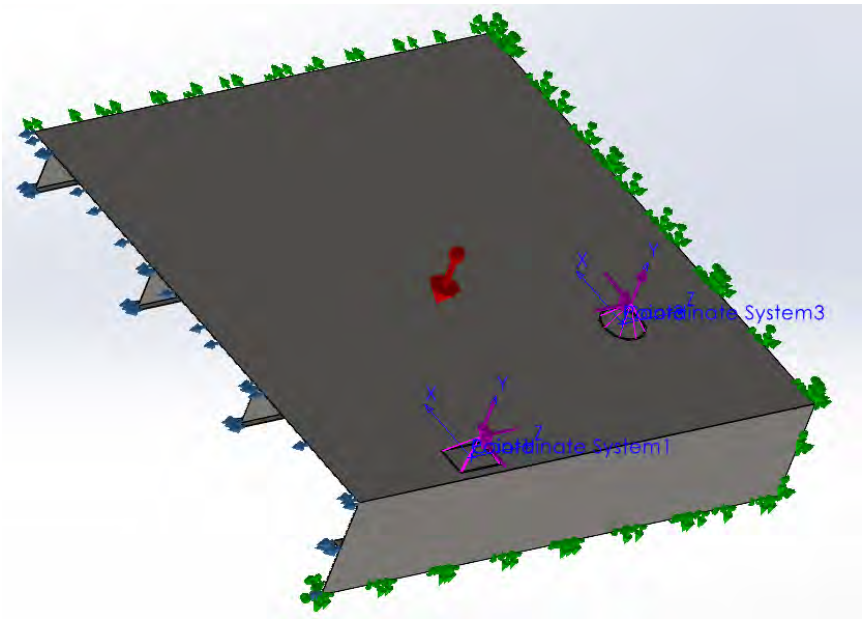

Figure 5. 11 Symmetry Fixture in blue color

3. Roller/Slider Fixture

The Roller/Slider fixture in SOLIDWORKS simulation restricts the degree of freedom which is normal to the plane where the fixture is applied. It is only applicable to planar faces and similar to the symmetry fixture, it reduces stress concentration at the area where it is applied and provokes torque development. [48]

For this model, Roller/Slider fixture is used at the last transverse frame and the right side of the section. (Figure 5.12)

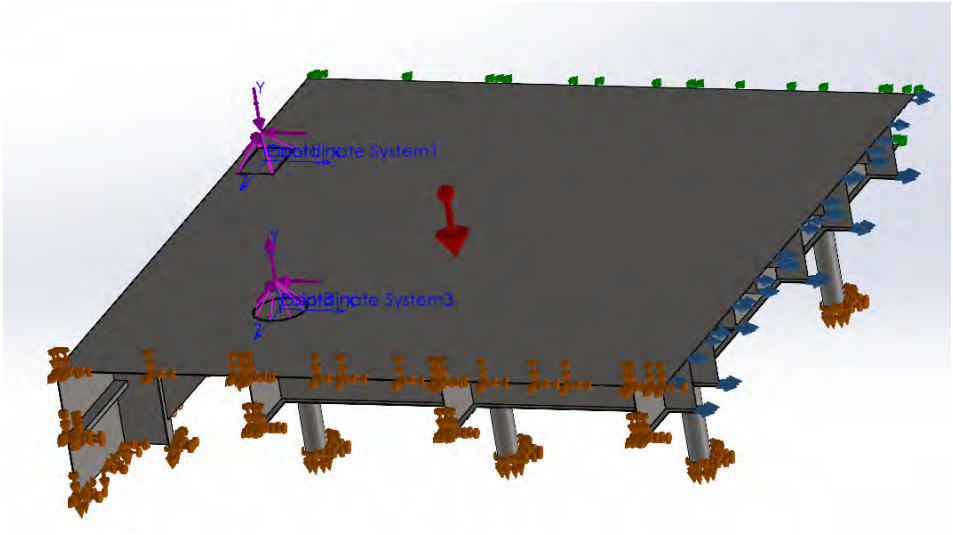

Figure 5. 12 Roller Slider Fixture indicated in blue color.

5.2.2 Loads

The most common steel materials used for hull structures are mild steel, AH 32, and AH 36. Each of them has a different yield strength (σ_y). Specifically, the allowable stresses are presented in Table 6.

Table 6 Allowable Stresses

Item	Allowable Stress		
Direct stress (Normal stress)	Yield Strength (σy) of the material	Mild Steel	235 MPa
		AH 32	315 MPa
		AH 36	355 MPa

The safe working load (SWL) for the mooring fittings was approved by the classification society. Therefore, the SWL applied to the closed chock is indicated in the AutoCAD design (Figure 5.12)

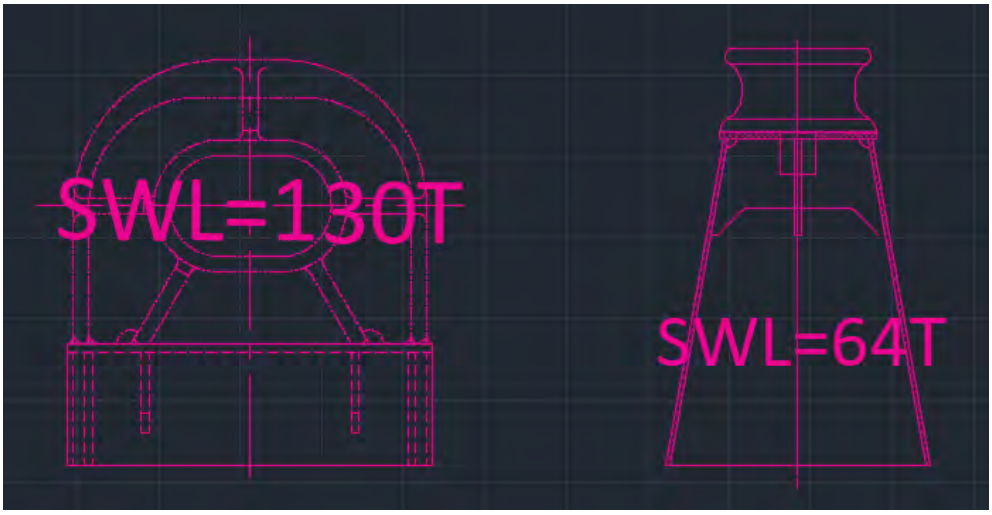

Figure 5. 13 Safe Working Load of the closed chock and the roller (right)

Moreover, the load case presented in the current simulation follows the direction of the rope directions shown in Figure 5.2.

In order to place the implemented loads on SOLIDWORKS Simulation, the forces needed to be analyzed in the longitudinal and lateral axes (x, y). The Force analysis is depicted in Figure 5.13.

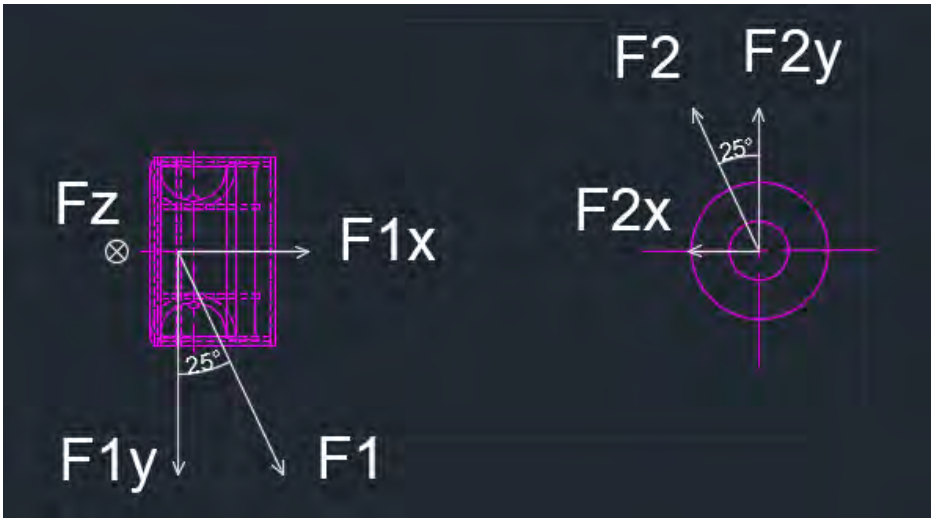

Figure 5. 14 Mooring Forces Analysis

Three load cases of rope directions are used when the chocks are tested in the marine industry for durability. However, for this particular test, we will only apply the

condition where the rope direction is 90º downwards since it is proven to be the most harmful for the deck as well as the fitting.

The Forces presented in Figure 5. , are distributed below.

- F_1 = 9.81 (m/s^2) * 64 (T) * 1000 (kg/T) = 627840 N
- F_{1x} = 627840 * sin(25 º) = 265336 N
- F_{1y} = 627840 * cos(25 º) = 569016 N
- $F_2 = F_1$ = 627840 N
- $F_{2x} = F_{1x}$ = 265336 N
- $F_{2y} = F_{1y}$ = 569016 N
- F_z = 9.81 * 130 * 1000 = 1275300 N

The safety factor used for studying mooring fittings is equal to 1.25 according to the IACS Common Structural Rules. Therefore, each force should be multiplied by this value:

- F_{1x} = 265336 *1.25 = 331670 N
- F_{1y} = 569016 *1.25 = 711270 N
- $F_{2x} = F_{1x}$ = 331670 N
- $F_{2y} = F_{1y}$ = 711270 N
- F_z = 1275300 *1.25 = 1594125 N

The loads above were inserted in the finite element analysis in their correspondent fitting. They were applied as distributed loads at a reference coordinate system that resembled each mooring equipment.

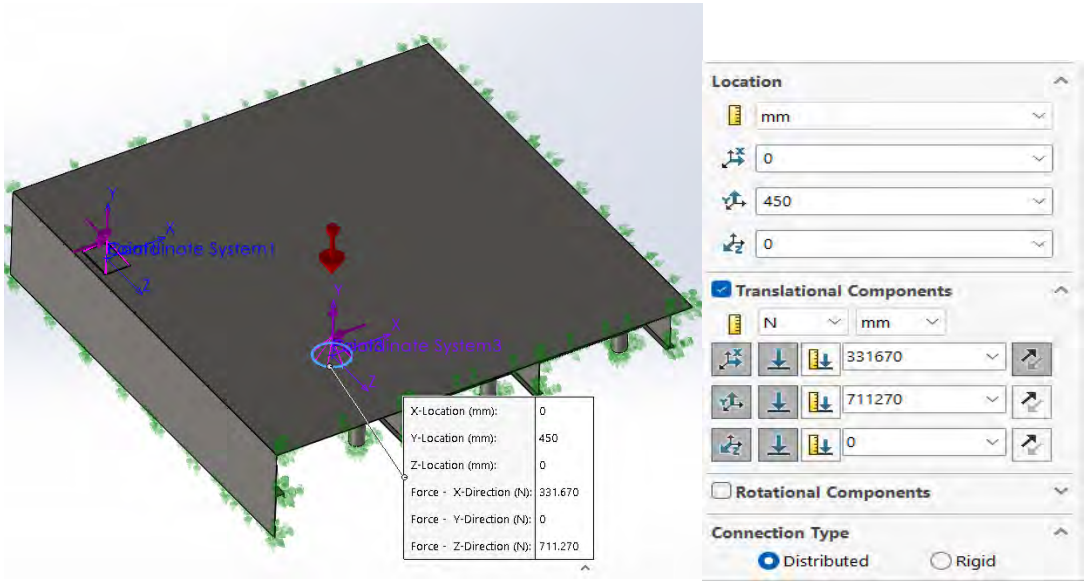

Figure 5. 15 Loads appliance on the capstan roller

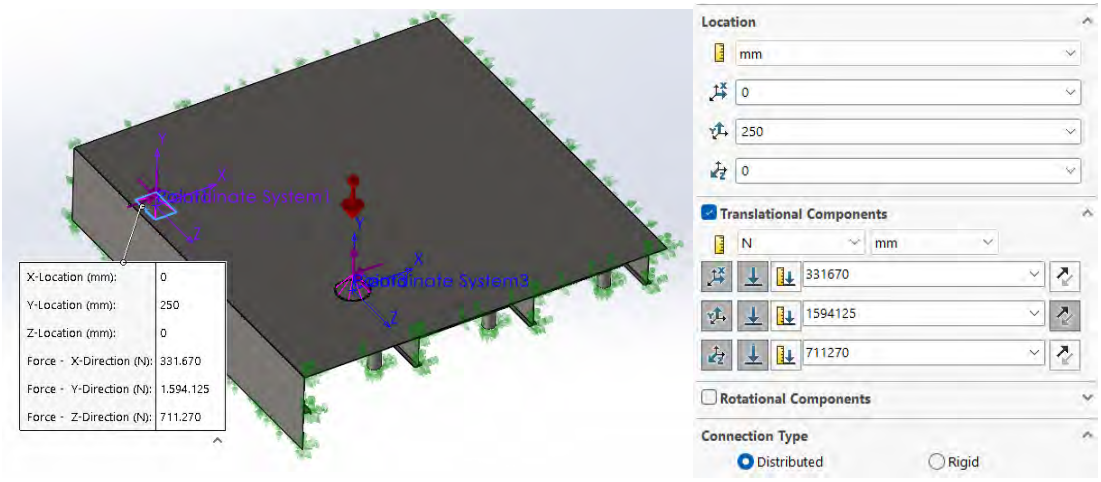

Figure 5. 16 Loads appliance on the deck mounted chock

Furthermore, distributed mass was applied according to the given weight of the chock and the roller (Figure 5.16 and Figure 5.17).

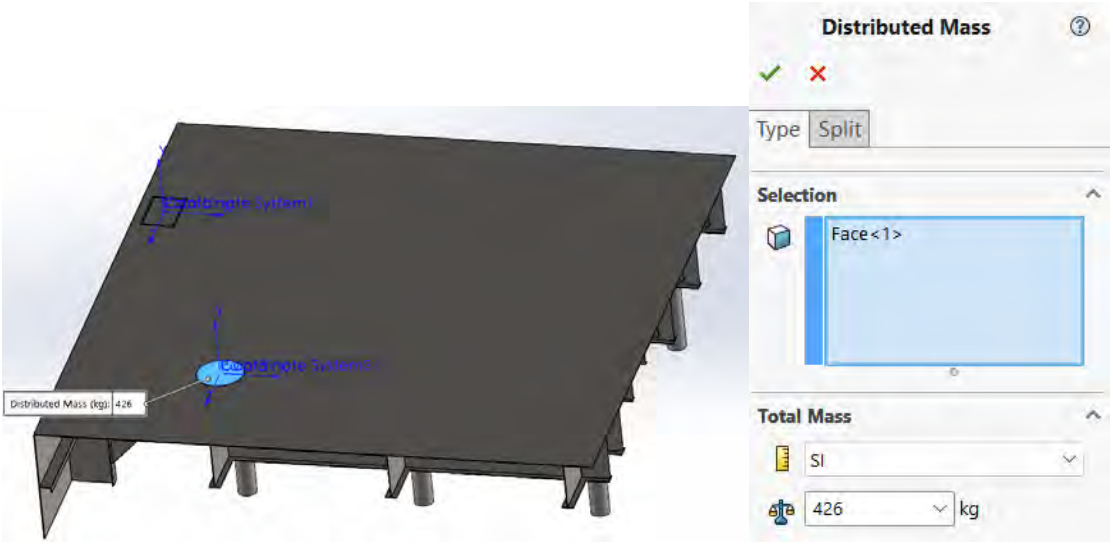

Figure 5. 17 Weight distribution on the capstan roller

Figure 5. 18 Weight distribution on the deck-mounted chock

Finally, gravity needed to be distributed.

5.2.3. Meshing

Meshing is of vital importance for the simulation process. Even though SolidWorks automatically generates the mesh for the 3D model, certain parameters needed to be modified to fit the geometry of the deck and for achieving more accurate results.

Generally, SOLIDWORKS has three options for mesh development.

- Standard mesh
- Curvature-based mesh

- Blended curvature-based mesh

For this study, a curvature-based mesh is chosen, because contrary to the standard mesh, it creates automatically more elements at regions where the surface is curved and consequently helps the user avoid the appliance of control mesh. Meanwhile, blended curvature was not selected due to its demand for high computational power and excessive time consumption.

When it comes to mesh element type, two-dimensional triangular shell elements were chosen because they are naturally suitable for structures made from metal plates and have thin features, like the deck simulated in this study. Conversely, 3D tetrahedral solid elements are well-suited for rough-cut and bulky constructions.

There is a fine line considering the density of the mesh elements. It should be set in order to give accurate results while being relatively computationally easy. The finer the elements are, the more precise the results will be, but, at the same time, the simulation becomes more time-consuming. For the particular model, the element size chosen is a maximum of 100mm and a minimum of 10mm, the minimum number of elements in a circle is 8 and the element growth ratio is 1.4. (Figure 5.18)

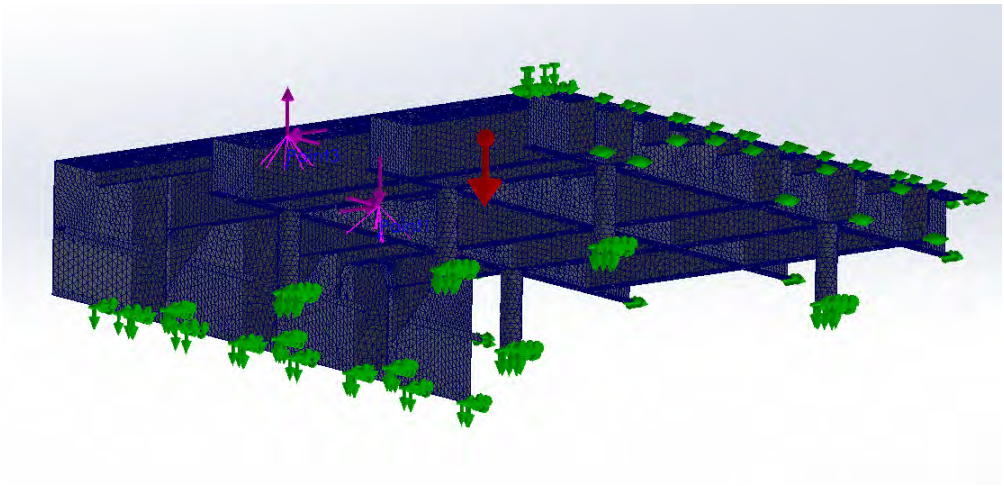

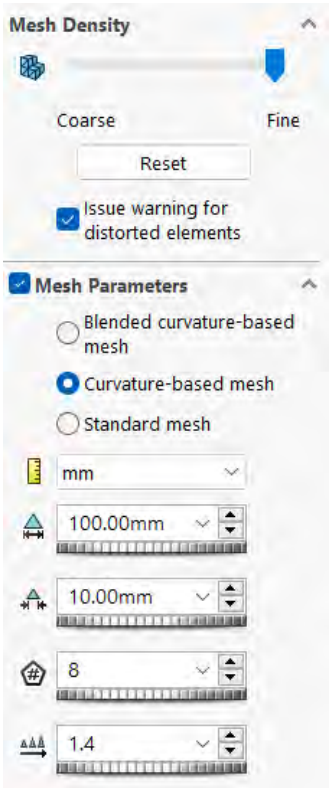

Figure 5. 19 Mesh parameters for the designed deck

5.3 Results

After meshing the model and running the study, stresses and displacement were calculated. In particular, in Figure 5.19 the results of the developed Von Misses stresses are presented. As indicated, the stresses are concentrated around the fittings, while the maximum annotations are at the underdeck stiffeners. This fact can be easily identified through the SOLIDWORKS command, “Iso Clipping”, which shows the areas of the structure that receive stresses above the input value. Namely, in Figure

5.20 the areas receiving stresses above 110 MPa are depicted. It is clear that the maximum developed stress is 219 MPa which according to Table 6 is below the allowable stress (σy) of all, Mild Steel (σy = 235 MPa), AH 32 (σy = 315 MPa), AH 36 (σy = 355 MPa). Thus, the structure complies with the safe operation rules.

Item	Allowable Stress		
Direct stress (Normal stress)	Yield Strength (σy) of the material	Mild Steel	235 MPa
		AH 32	315 MPa
		AH 36	355 MPa

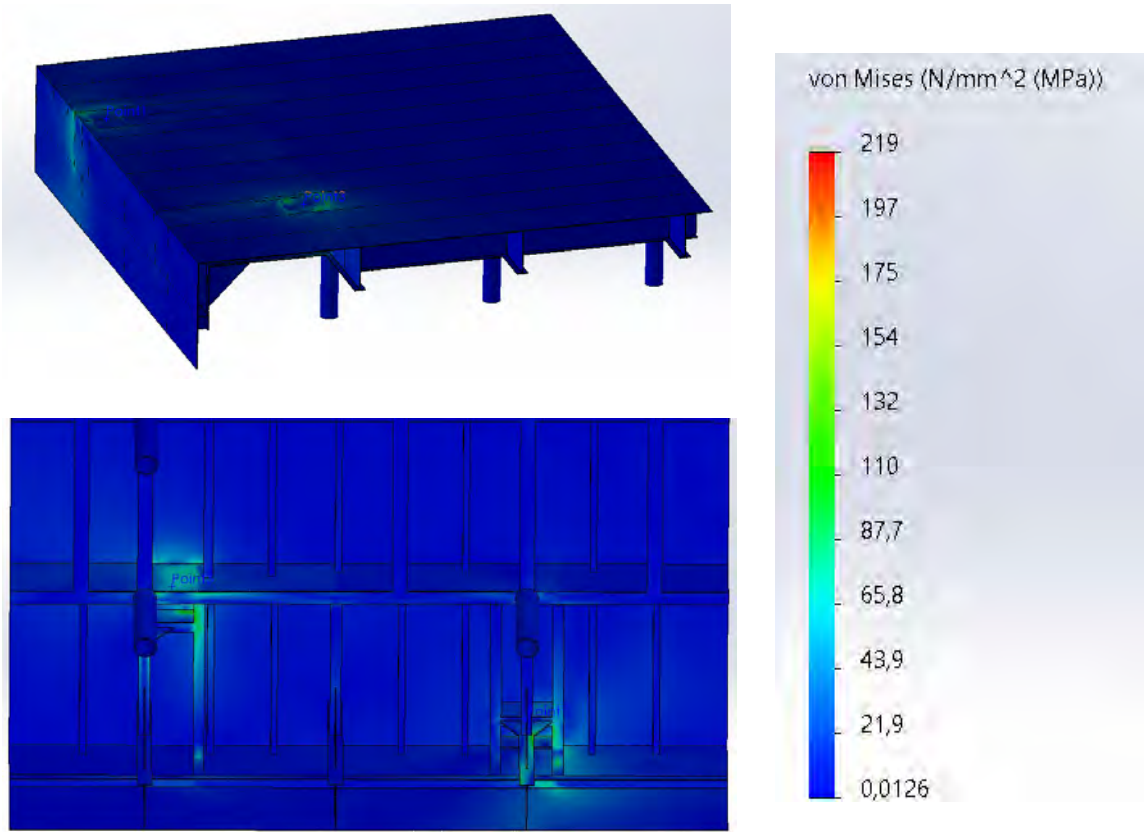

Figure 5. 20 Developed Stresses in MPa

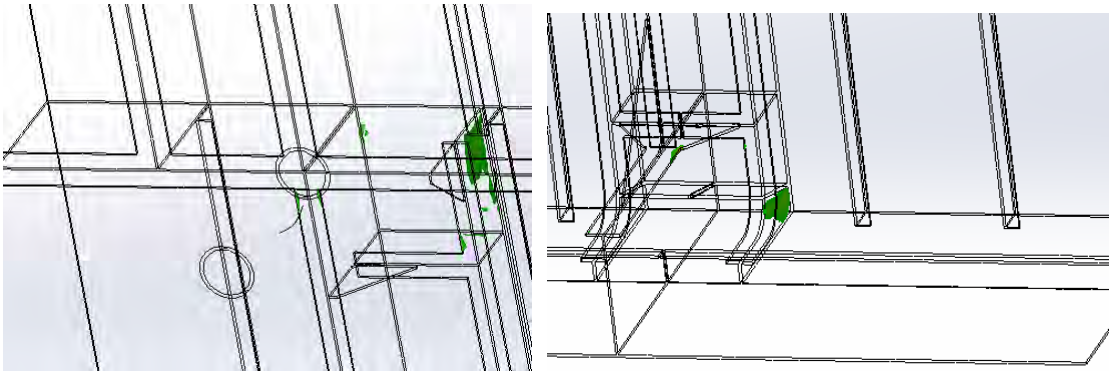

Figure 5. 21 Max Annotations under the mooring fittings

Furthermore, the displacement results are shown in Figure 5.21, and they are obviously insignificant in comparison with the size of the structure since the maximum displacement is 1.648mm.

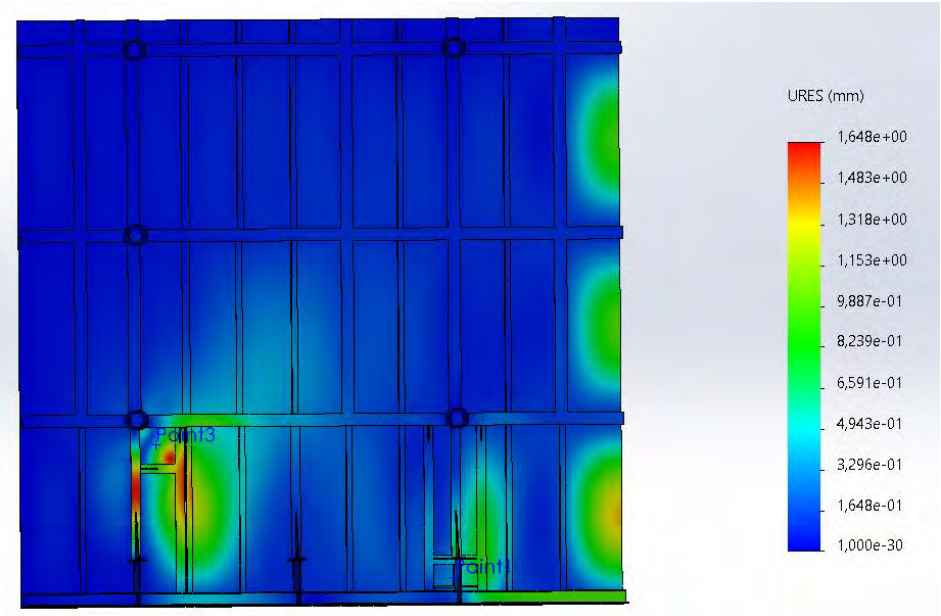

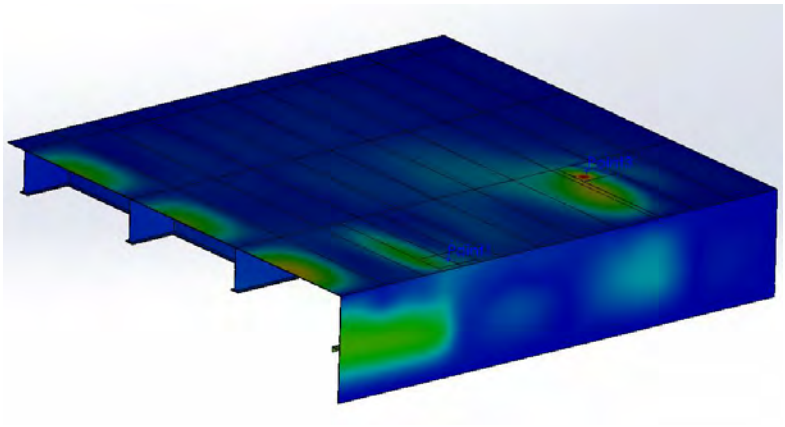

Figure 5. 22 Displacement Results

5.4 Experiment with corrosion addition.

The vessel was built according to the Common Structural Rules that the classification Society has determined. Hence, the regulations that appertain corrosion are in accordance with the IACS rules.

IACS (International Association of Classification Societies) is based on the foundation of maritime knowledge and technology, a Classification Society ("CS") provides approval, statutory certification, and services as a Recognized Organization acting on behalf of a flag administration. It also assists the maritime industry and regulatory bodies concerning maritime safety and pollution prevention.

Corrosion allowance diversifies in different types of ships and different parts of the vessel. It depends on the environmental condition the component is exposed to, its thickness, and its function.

The survey has been conducted in compliance with the IACS common structural rules 2023. Meanwhile, the thickness loss has been calculated from Part 1, Chapter 3, and Section 3 of the regulation booklet and it is modeled as general corrosion.

The corrosion addition (t_c) to the existing plating thickness is calculated using the Table and the following equation.

$$t_c = Roundup_{0.5}(t_{c1} + t_{c2}) + t_{res} \quad [mm]$$

Where:

- t_{c1} and t_{c2} are allowable diminution thicknesses on each side of the considered structural surface and they are indicated in Table 7

- t_{res} is the reserved thickness which is considered approximately 0.5mm.

Table 7 Corrosion Additions

Compartment type	Structural member		t_{c1} or $tc2$		
			Oil tankers	BC-A or BC-B ships with $L_{LL} \geq 150$ m	Other BC ships
Ballast water tank, bilge tank, drain storage tank, chain locker [1]	Face plate of PSM	Within 3m below top of tank [4]	2.0		
		Elsewhere	1.5		
	Other members [2] [3]	Within 3m below top of tank [4]	1.7		
		Elsewhere	1.2		
Cargo oil tank, slop tank	Face plate of PSM	Within 3m below top of tank [4]	1.7	N/A	
		Elsewhere	1.4		
	Inner-bottom plating/bottom of tank		2.1		
	Other members	Within 3m below top of tank [4]	1.7		
		Elsewhere	1.0		
Dry bulk cargo hold [5]	Transverse bulkhead	Upper part [6]	N/A	2.4	1.0
		Lower stool: sloping plate, vertical plate and top plate [7]		5.2	2.6
		Other parts		3.0	1.5
	Sloped plating of hopper tank, inner bottom plating			3.7	2.4
	Other members	Upper part [6]		1.8	1.0
		Webs and flanges of the upper end brackets of side frames of single side bulk carriers			
		Webs and flanges of lower brackets of side frames of single side bulk carriers		2.2	1.2
		Other parts		2.0	1.2
Exposed to atmosphere	Weather deck plating		1.7		
	Other members		1.0		

Compartment type	Structural member	t_{c1} or $tc2$		
		Oil tankers	BC-A or BC-B ships with $L_{LL} \geq 150$ m	Other BC ships
Exposed to seawater	Shell plating between the minimum design ballast draught waterline and the scantling draught waterline	1.5		
	Shell plating elsewhere	1.0		
Fuel and lube oil tank		0.7		
Fresh water tank		0.7		
Void spaces [8]	Spaces not normally accessed, e.g. access only via bolted manhole openings, pipe tunnels, inner surface of stool space not common with a dry bulk cargo hold or ballast cargo hold, etc.	0.7		
Dry spaces	Internals of machinery spaces, pump room, store rooms, steering gear space, etc.	0.5		

(1) 1.0 mm is to be added to the plate surface within 3m above the upper surface of the chain locker bottom.

(2) 0.5 mm is to be added to the plate surface exposed to ballast for the plate boundary between water ballast and heated cargo oil tanks/slop tanks. 0.3mm is to be added to each surface of the web and face plate of a stiffener in a ballast tank and attached to the boundary between water ballast and heated cargo oil tanks or heated fuel/lube oil tanks/slop tanks. Heated oil tanks are defined as tanks/slop tanks arranged with any form of heating capability (the most common type is heating coils).

(3) 0.7 mm is to be added to the plate surface exposed to ballast for the plate boundary between water ballast and heated fuel oil or lube oil tanks.

(4) Only applicable to cargo tanks/slop tanks and ballast tanks with weather deck as the tank top. The 3 m distance is measured vertically from and parallel to the top of the tank.

(5) Dry bulk cargo hold includes holds intended for the carriage of dry bulk cargoes, which may carry water ballast.

(6) Upper part of the cargo holds correspond to an area above the connection between the topside and the inner hull or side shell. If there is no topside, the upper part corresponds to the upper one third of the cargo hold height (where a plane bulkhead is fitted in way of a dry bulk cargo hold, the upper part of the bulkhead is defined in the same manner).

(7) If there is no lower stool fitted (i.e. engine room bulkhead or fore peak bulkhead) or if a plane bulkhead is fitted, then this corrosion addition should be applied up to a height level with the opposing bulkhead stool in that hold. In the case where a stool is not fitted on the opposing bulkhead, the vertical extent of this zone is to be from the inner bottom to a height level with the top of the adjacent hopper sloping plate, but need not be taken as more than 3 m.

(8) For the determination of the corrosion addition of the outer shell plating, the pipe tunnel is considered as for a water ballast tank.

In this particular case, the corrosion additions driven by the Table are:

- For webs and flanges of under-deck stiffeners: tc1 = tc2 = 0.5mm

(Under the main upper deck there are dry spaces used for storage according to the structural designs)

- For deck plating: tc1 = tc2 = 1.7mm

(The upper deck is exposed to the atmosphere)

- For the bulwark at Frame -7: tc1 = tc2 = 2.4mm

The reduction thicknesses are calculated below:

- For webs and flanges of under-deck stiffeners:

$$t_c = Roundup_{0.5}(0.5 + 0.5) + 0.5 = 1.5 + 0.5 = 2\ mm$$

t_c= 2 mm

- For deck plating:

$$t_c = Roundup_{0.5}(1.7 + 1.7) + 0.5 = 4 + 0.5 = 4.5\ mm$$

t_c= 4.5 mm

- For bulwark at Frame -7:

$$t_c = Roundup_{0.5}(2.4 + 2.4) + 0.5 = 5 + 0.5 = 5.5\ mm$$

t_c= 5.5 mm

5.4.1 Simulation Process on the Corroded Deck

After the 3D design with diminished thicknesses, the structure was modeled for FEA Simulation similarly to the non-corroded one (Figure 5.22). Hence, the fixtures, the mesh parameters, and the loads are the same as above.

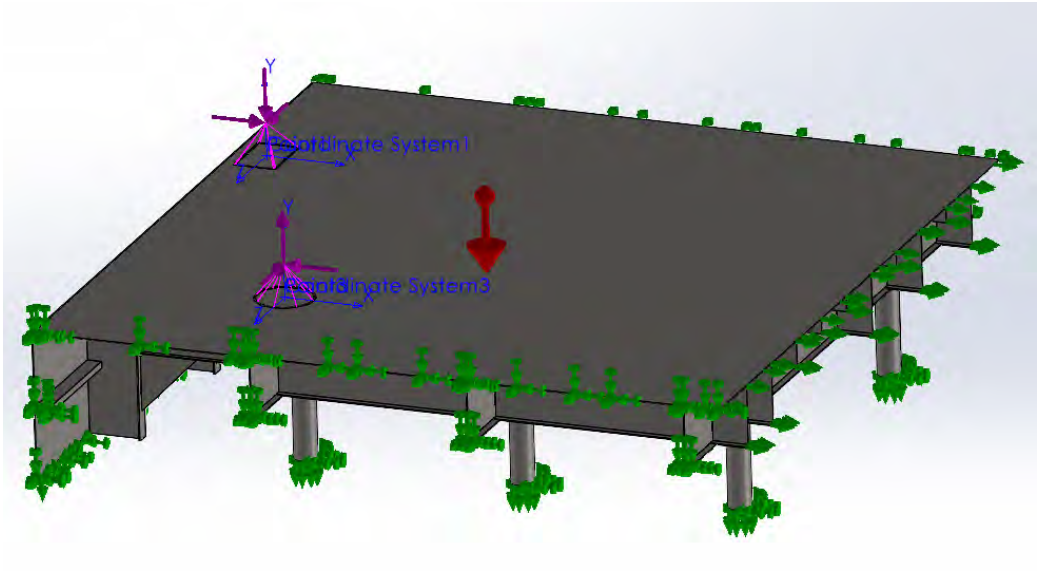

Figure 5. 23 FEA Modeling

The results of the simulation are indicated in Figure 5.23, where it is visible that the stresses are concentrated around the mooring fittings. Clearly, it appears that the stresses are larger after the corrosion addition. The value 697 MPa, however, seems to be a false number and has most certainly been provoked due to an abnormality in the geometry of the 3D model. This phenomenon sometimes occurs in FEA Simulations and is known as a 'Hot Spot', or singularity. It can be easily detected because all the high stresses are concentrated in a very small region, almost equal to the meshing element (Figure 5.24). The true results are presented in Figure 5.25 by using Iso Clipping. It is obvious that stresses above 300 MPa are developed and can reach up to 355 MPa. Thus, these results prove that the generated stresses exceed the allowable ones indicated in Table 6. Even the AH 36 steel, which has higher strength, is at risk for fracture.

Therefore, additional reinforcements should be added to the deck in order to ensure safety. The supplemental structure, though, would be some extra brackets or thicker plating to some added stiffeners, because the region suffering from stresses above 300 MPa is limited.

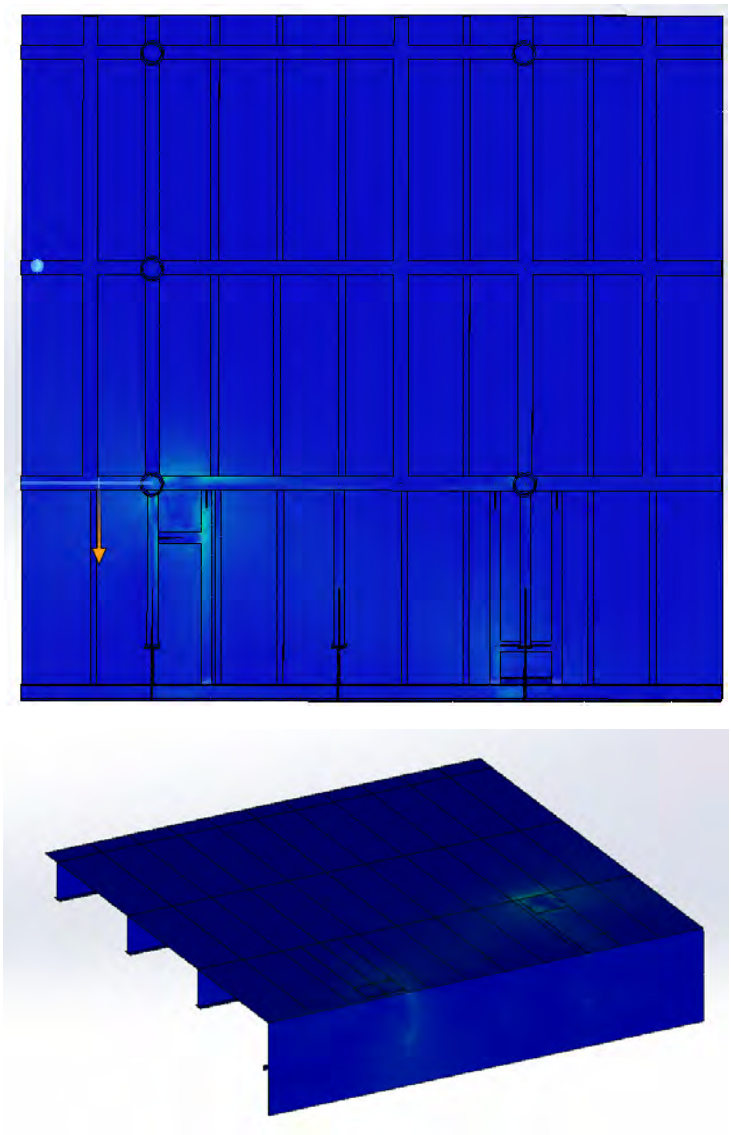

Figure 5. 24 Stresses results of the corroded model

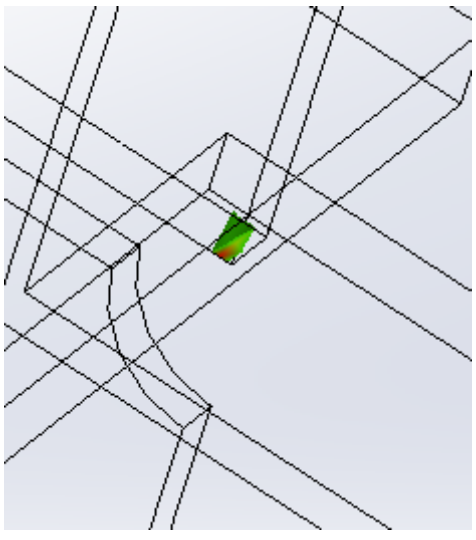

Figure 5. 25 Stresses above 400 MPa

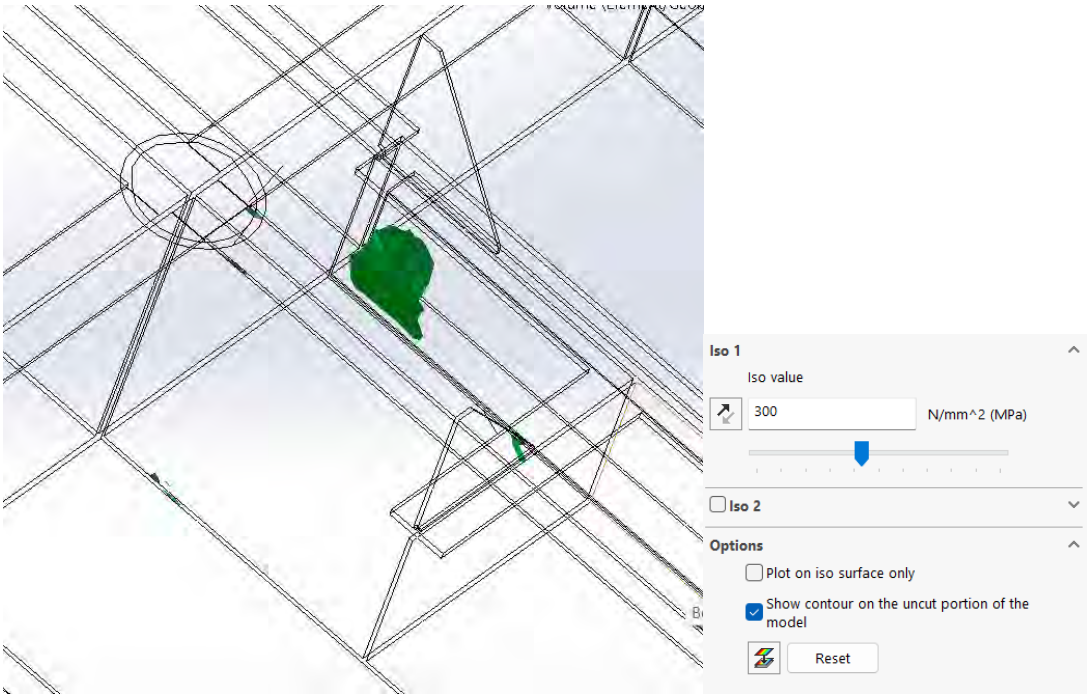

Figure 5. 26 Regions receiving stresses above 300 MPa.

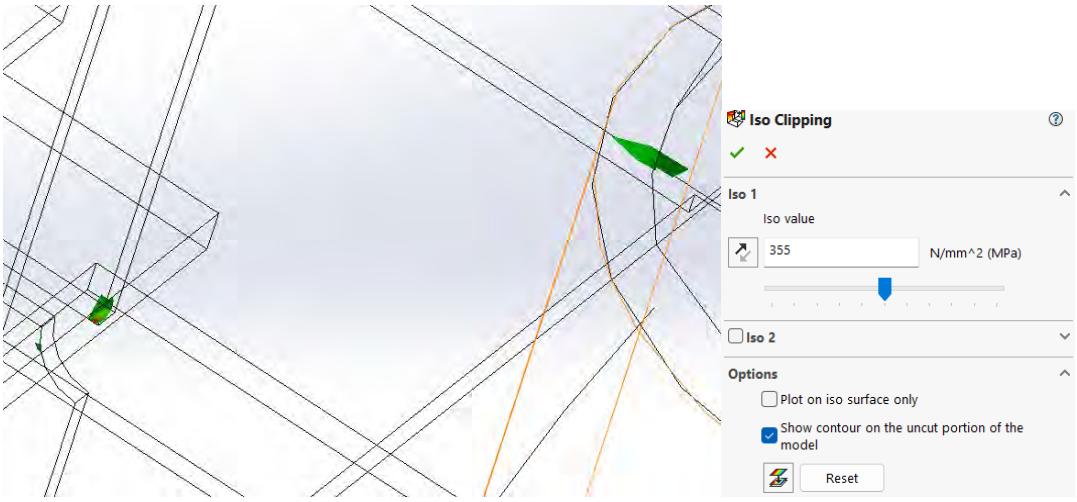

Figure 5. 27 Regions receiving stresses above 355 MPa.

Finally, the displacement results are presented in Figure 5.26, where the maximum value, 3.848 mm, is clearly larger than the one of the non-corroded model, 1.648 mm.

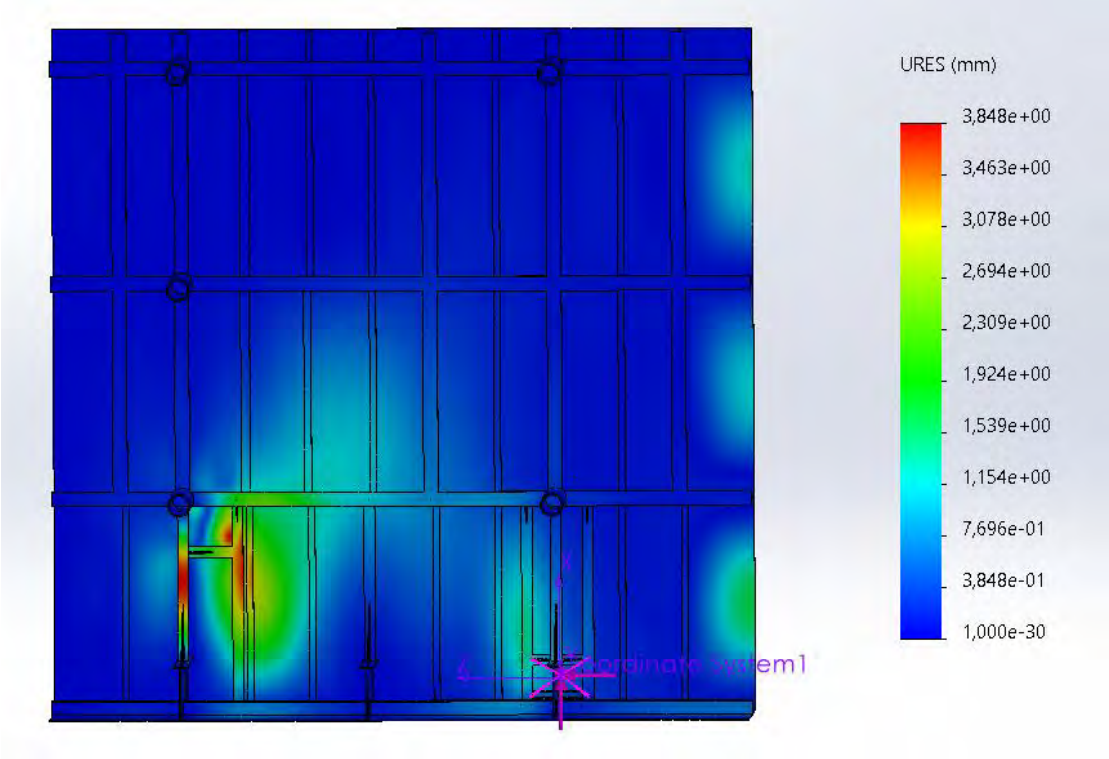

Figure 5. 28 Displacement results of corroded deck

The comparison of the stresses and displacement results between the initial and intact structure and the corroded model is presented in Table 8.

Table 8 Results comparison

	Maximum Stresses (MPa)	Maximum Displacement (mm)
Before Corrosion	219	1,648
After Corrosion	>355	3,848

5.5 Observations

To conclude, when the structure is corroded, the stresses that are generated are significantly larger than the ones in the initial structure. Thus, even though the decreased thicknesses comply with the allowable corrosion addition, it is proven that the steel plating can be easily deformed, and therefore damaged, since the stresses exceed the acceptable, jeopardizing the safety of the vessel and the mooring operation.

Chapter 6: Conclusions

After conducting a comprehensive literature review, several key insights regarding the impact of corrosion on structures exposed to marine environments were discerned.

- The maritime industry is significantly affected by corrosion, leading to repercussions in economic, energy conservation, environmental, and human safety aspects.
- The marine environment can be highly corrosive due to its properties. Specifically, the salinity of seawater is influenced by its chloride ion content. As the salt content in the water increases, so does its conductivity, leading to greater corrosive potential. Moreover, the dissolved oxygen concentration is a crucial factor that further amplifies the mechanism as the quantity increases. In addition, elevated temperatures generally expedite the corrosion process due to the acceleration of chemical reactions and the increased kinetic energy of the sea molecules, but also because heightened temperatures contribute to the increase in microbial activity. The water flow velocity is an aspect that contributes to this phenomenon due to the initiation of cavitation and erosion-corrosion that are especially dangerous for the metal surface. Lastly, the variation of immersion depth affects the development of corrosion damage differently. It has been proven that corrosion is most aggressive in the splash zone.
- Structures and vessels exposed to the sea are prone to corrosion, leading to weakening and degradation of the steel and potential fracture. The shipping industry most commonly experiences atmospheric, galvanic, microbial, flow-accelerated corrosion (FAC), erosion-corrosion, and cavitation. Firstly, atmospheric corrosion is a significant factor to take into account, even though the vessel is not fully immersed in the sea. In the seawater atmosphere humidity is culpable for the formation of a thin aqueous film on the metal surface, which serves as an electrolyte and triggers corrosion. This moisture layer typically contains salts and pollutants, transferred through the wind. Flow-accelerated corrosion is a particularly prominent form of corrosion in the shipbuilding industry, primarily affecting carbon steel. This is due to the inability to form a passive layer on the metal surface, attributed to the constant relative motion of water with the metal. Erosion corrosion acts similarly as it is generated in high

flow velocities but it also involves the submontane effect and collision of abrasive particles carried by the water. Meanwhile, cavitation, a form of erosion-corrosion is more frequent in accelerated and turbulent flows, where the pressure and velocity are not constant. This fluctuation in pressure facilitates the development of cavities and bubbles, which collapse on the steel surface with an increase in pressure and erode the material. Galvanic corrosion is a common occurrence in maritime settings, resulting from the contact of two dissimilar metals that form an anode-cathode pair based on their electronegativity. In this process, the seawater serves as the electrolyte and facilitates an electrochemical reaction, ultimately leading to significant corrosion due to the environmental conditions.

- These factors collectively contribute to the highly corrosive nature of the maritime conditions and the accelerated deterioration of the structures, making corrosion prevention and protection essential considerations in marine engineering and infrastructure design. Corrosion can be effectively prevented from the early stages of the design process through the utilization of high-quality, well-prepared materials. An essential maintenance method is cathodic protection, which comes in two types: sacrificial anodes and impressed current. Sacrificial anodes, found in galvanic cathodic suppression systems, consist of a metal that is more reactive than the ship's hull. Meanwhile, the impressed current method requires an external power source to generate electric current. A regular process is protection through paint which impedes the ship’s hull exposure to the corrosive environment.
- Furthermore, the FEA simulation indicated that corrosion leads to structural weakening and degradation of steel, ultimately jeopardizing the safety of vessels and mooring operations. This is substantiated by the analysis of stresses and displacement results, which demonstrate a significant increase in both stress levels and displacement values in corroded structures compared to their non-corroded counterparts. Namely, the maximum stress levels and displacement values observed post-corrosion exceed those of the initial, non-corroded structure.

In conclusion, the thesis highlights the necessity for measures to mitigate the destructive effects of corrosion in marine conditions. The significance of regular

inspections, research, and advancements in corrosion prevention and protection strategies should be emphasized, in order to secure naval integrity, longevity, and safety in the operations of maritime structures and vessels. Besides, regulations are constantly renewed due to new surveys and research. The shipbuilding industry is evolving rapidly and innovative ideas and solutions are presented.

Corrosion in Marine Structures

Chapter 7: Bibliography

1. Antonios K. Tasiopoulos, "Η ΔΙΑΒΡΩΣΗ ΤΩΝ ΔΕΞΑΜΕΝΩΝ ΦΟΡΤΙΟΥ (CARGO HOLDS) ΤΩΝ ΦΟΡΤΗΓΩΝ ΠΛΟΙΩΝ ΜΕΤΑΦΟΡΑΣ ΞΗΡΟΥ ΦΟΡΤΙΟΥ ΧΥΔΗΝ (BULK CARRIERS)"
2. Gregory Haidemenopoulos Notes, 'Corrosion'
3. Nace International. "ASSESSMENT OF THE GLOBAL COST OF CORROSION," 2016. http://impact.nace.org/economic-impact.aspx.
4. Corrosion science and engineering information hub. "Corrosion Cost to Society." Corrosion Doctors. https://corrosion-doctors.org/Principles/Cost.htm.
5. Νικόλαος Χαιδεμενόπουλος, Πάνος Καπασάκης, "Επισκόπηση της Διάβρωσης σε Πλοία και Εγκαταστάσεις του Ελληνικού Πολεμικού Ναυτικού"
6. Fossier, Brittany. "THE EFFECTS OF CORROSION IN THE MARINE INDUSTRY." Fibergate Composite Structures, Jun. 19, 2014. https://blog.fibergrate.com/blog/the-effects-of-corrosion-in-the-marine-industry.
7. Javaherdashti, Reza. "How Corrosion Affects Industry and Life." Anti-Corrosion Methods and Materials, no. 1 (February 1, 2000): 30–34. https://doi.org/10.1108/00035590010310003.
8. Zakowski, K., M. Narozny, M. Szocinski, and K. Darowicki. "Influence of Water Salinity on Corrosion Risk—the Case of the Southern Baltic Sea Coast." Environmental Monitoring and Assessment, no. 8 (April 3, 2014): 4871–79. https://doi.org/10.1007/s10661-014-3744-3.
9. Zakiah, Diah, Yuni Mariah, Deny Fitrial, and Asman Ala. "An Analysis on Influence of Sea Water Salinity and Acidity in Jakarta Ports Towards Corrosion Rate of Steel Plate as Ship Material." Proceedings of the Proceedings of the 1st International Conference on Management, Business, Applied Science, Engineering and Sustainability Development, ICMASES 2019, 9-10 February 2019, Malang, Indonesia, 2020. https://doi.org/10.4108/eai.3-8-2019.2290735.
10. Valdez, Benjamin, et al. "The Influence of Minerals on Equipment Corrosion in Geothermal Brines ." Area of Chemical Engineering Materials, Minerals and Corrosion Department , Universidad Autonoma de Baja California .
11. Cox, G. L., and B. E. Roetheli. "Effect of Oxygen Concentration on Corrosion Rates of Steel and Composition of Corrosion Products Formed in Oxygenated Water." Industrial & Engineering Chemistry, no. 9, American Chemical Society (ACS), Sept. 1931, pp. 1012–16. Crossref, doi:10.1021/ie50261a011.
12. Yan, Xuanqi, et al. "Research Progress on Factors Affecting Oxygen Corrosion and Countermeasures in Oilfield Development." E3S Web of Conferences, edited by Z.B. Xu et al., EDP Sciences, 2019, p. 01031. Crossref, doi:10.1051/e3sconf/201913101031.

13. Li, Zhen, et al. “The Influence of Critical Flow Velocity on Corrosion of Stainless Steel.” Journal of Failure Analysis and Prevention, no. 6, Springer Science and Business Media LLC, Oct. 2017, pp. 1234–40. Crossref, doi:10.1007/s11668-017-0369-1.
14. Xu, Yunze Xu, and Qiliang Zhang Zhang. “Flow Accelerated Corrosion and Erosion−corrosion Behavior of Marine Carbon Steel in Natural Seawater.” Journal of Failure Analysis and Prevention.
15. Guedes Soares, Carlos, and Yordan Garbatov. “Effect of Environmental Factors on Steel Plate Corrosion under Marine Immersion Conditions.” Corrosion Engineering, Science and Technology, no. 4, SAGE Publications, June 2011, pp. 524–41. Crossref, doi:10.1179/147842209x12559428167841.
16. Ganz, Stephen Ganz. Cavitation : Causes , Effects , Mitigation and Application. 2012.
17. Farro, N. W., et al. “Copper Marine Corrosion: I. Corrosion Rates in Atmospheric and Seawater Environments of Peruvian Port.” The Open Corrosion Journal, no. 1, Bentham Science Publishers Ltd., Apr. 2009, pp. 130–38. Crossref, doi:10.2174/1876503300902010130.
18. Bhandari, Jyoti, et al. “Modelling of Pitting Corrosion in Marine and Offshore Steel Structures – A Technical Review.” Journal of Loss Prevention in the Process Industries, Elsevier BV, Sept. 2015, pp. 39–62. Crossref, doi:10.1016/j.jlp.2015.06.008.
19. Guedes Soares, Carlos, and Yordan Garbatov. “Effect of Environmental Factors on Steel Plate Corrosion under Marine Immersion Conditions.” Corrosion Engineering, Science and Technology, no. 4, SAGE Publications, June 2011, pp. 524–41. Crossref, doi:10.1179/147842209x12559428167841.
20. “Microbiologically Influenced Corrosion (MIC) - Facts — Alleima.” Alleima, https://www.alleima.com/en/technical-center/corrosion/wet-corrosion/microbiologically-influenced-corrosion-mic/.
21. Joint, Ian, and Dan A. Smale. “Marine Heatwaves and Optimal Temperatures for Microbial Assemblage Activity.” FEMS Microbiology Ecology, edited by Riks Laanbroek, no. 2, Oxford University Press (OUP), Dec. 2016, p. fiw243. Crossref, doi:10.1093/femsec/fiw243.
22. Byron, FranK. “Corrosion Impact of Offshore Platforms, Structures, and Vessels.” Materials Performance Magazine, https://materialsperformance.com/articles/corrosion-basics/2020/12/corrosion-impact-of-offshore-platforms-structures-and-vessels. Accessed 6 Nov. 2023.
23. Khodabux, Waseem, et al. “Profiling Corrosion Rates for Offshore Wind Turbines with Depth in the North Sea.” Energies, no. 10, MDPI AG, May 2020, p. 2518. Crossref, doi:10.3390/en13102518.

24. **"Corrosion Classifications for Offshore Wind."** Https://Www.Onropes.Co.Uk/Corrosion-Classifications, Dangle Rope Access, 5 May 2020.

25. **Chen, Zhiwei, et al. "Corrosion Behavior of Marine Structural Steel in Tidal Zone Based on Wire Beam Electrode Technology and Partitioned Cellular Automata Model - ScienceDirect." ScienceDirect.Com | Science, Health and Medical Journals, Full Text Articles and Books.,** https://www.sciencedirect.com/science/article/pii/S2667266922000299

26. **Xu, Yong, et al. "Study on Corrosion Behavior and Mechanism of AISI 4135 Steel in Marine Environments Based on Field Exposure Experiment - ScienceDirect." ScienceDirect.Com | Science, Health and Medical Journals, Full Text Articles and Books.,** https://www.sciencedirect.com/science/article/pii/S004896972201957X. Accessed 13 Nov. 2023.

27. **Jenifer Alcántara, et al. "Marine Atmospheric Corrosion of Carbon Steel: A Review - PMC." PubMed Central (PMC),** https://www.ncbi.nlm.nih.gov/pmc/articles/PMC5506973/.

28. **C. Guedes Soares, et al. "Influence of Environmental Factors on Corrosion of Ship Structures in Marine Atmosphere - ScienceDirect." ScienceDirect.Com | Science, Health and Medical Journals, Full Text Articles and Books.,** https://www.sciencedirect.com/science/article/pii/S0010938X09002315?via=ihub.

29. **Engineering, Minicy Catom Software. "Marine." CORRIZONSG (International Corrosion Protecting Systems),** https://www.corrizonsg.com/marine.html.

30. **S.W. Dean. "Natural Atmospheres: Corrosion - ScienceDirect." ScienceDirect.Com | Science, Health and Medical Journals, Full Text Articles and Books.,** https://www.sciencedirect.com/science/article/pii/B0080431526010330

31. **Baigang AN, et al. "Corrosion and Runoff Behavior of Carbon Steel in Simulated Acid Rain."** https://citeseerx.ist.psu.edu/document?repid=rep1&type=pdf&doi=3854e54899e7acc206481e9725435c617e5fd75d

32. **Bahman Daneshian, et al. "Effect of Climatic Parameters on Marine Atmospheric Corrosion: Correlation Analysis of on-Site Sensors Data | Npj**

Materials Degradation." Nature, Springer Nature, https://www.nature.com/articles/s41529-023-00329-6.

33. Ivošević, Špiro, et al. "Probabilistic Estimates of Corrosion Rate of Fuel Tank Structures of Aging Bulk Carriers." International Journal of Naval Architecture and Ocean Engineering, no. 1, Elsevier BV, Jan. 2019, pp. 165–77. Crossref, doi:10.1016/j.ijnaoe.2018.03.003.

34. Gardiner, C. P., and R. E. Melchers. "Enclosed Atmospheric Corrosion in Ship Spaces." British Corrosion Journal, no. 4, Informa UK Limited, Oct. 2001, pp. 272–76. Crossref, doi:10.1179/000705901101501730.

35. 6.1 Upper Deck Areas. https://www.imorules.com/GUID-4C9631E3-3728-467A-AAA9-0CFE0AF83A69.html.

36. "Deck Fittings & Mooring Equipment – Lam Hong Group." Lam Hong Group – Marine & Offshore Supplies | Since 1946, https://www.lamhongs.com.sg/products/mooring.

37. "Towing Operations on Domestic Commercial Vessels." Australian Maritime Safety Authority, https://www.amsa.gov.au/vessels-operators/domestic-commercial-vessels/towing-operations-domestic-commercial-vessels.

38. Benavent, Herb. "Galvanic Corrosion on Your Mast — Rigging Doctor." Rigging Doctor, Rigging Doctor, 24 Jan. 2020, https://www.riggingdoctor.com/life-aboard/2020/1/14/galvanic-corrosion-on-your-mast.

39. Yunze Xu, et al. "Flow Accelerated Corrosion and Erosion−corrosion Behavior of Marine Carbon Steel in Natural Seawater | Npj Materials Degradation." Nature, Springer Nature, https://www.nature.com/articles/s41529-021-00205-1.

40. Σοφία Κ. Πέππα "Αντίσταση- Πρόωση- Υδροδυναμική πλοίου, Σπηλαίωση Ελίκων"

41. Carlton, John. Marine Propellers and Propulsion. Butterworth-Heinemann, 2012. http://www.maritimeexpert.files.wordpress.com

42. Suner, Munir, and Onur Birdal. "Effect of Cavitation in Ships on the Environment | SpringerLink." SpringerLink, Springer New York, 2013, https://link.springer.com/chapter/10.1007/978-1-4614-7588-0_51.

43. Hound, News. “An Introduction to Propeller Cavitation.” The International Institute of Marine Surveying (IIMS), 14 Jan. 2015, https://www.iims.org.uk/introduction-propeller-cavitation/.

44. Carlton, John. Marine Propellers and Propulsion. Butterworth-Heinemann, 2012. http://www.maritimeexpert.files.wordpress.com

45. Jonghyun Kim, and Joon Sang Lee. “Numerical Study of Cloud Cavitation Effects on Hydrophobic Hydrofoils - ScienceDirect.” ScienceDirect.Com | Science, Health and Medical Journals, Full Text Articles and Books., https://www.sciencedirect.com/science/article/abs/pii/S0017931014011594.

46. Yasmin Zein, Indah Aqnaita Tidar, et al. “Mooring Tension Analysis of the Effect of Mooring Configuration Variations When LNG Carrier Moored to a Jetty.” IOP Conference Series: Earth and Environmental Science, no. 1, IOP Publishing, Jan. 2022, p. 012023. Crossref, doi:10.1088/1755-1315/972/1/012023.

47. “Pedestal Fairlead - ISO13776 Roller Fairlead | YSmarines.” YSmarines, 12 July 2022, https://www.ysmarines.com/roller-fairlead/iso13776-pedestal-roller-fairlead/.

48. Jamie Hill. “Physics Fun with Jamie: SOLIDWORKS FEA Simulation Fixtures.” The Javelin Blog, https://www.facebook.com/JavelinTech, 27 Dec. 2022, https://www.javelin-tech.com/blog/2022/12/physics-fun-with-jamie-solidworks-fea-simulation-fixtures/.

49. William Mueller. “Basic Theory of Metallic Corrosion - Allied Corrosion Industries, Inc.” Allied Corrosion Industries, Inc., https://www.facebook.com/AlliedCorrosion, https://www.alliedcorrosion.com/basic-theory-of-metallic-corrosion/.

50. Pedeferri P., Lazzari L., Pedeferri M.; (2018) “Corrosion science and engineering”, Springer, Italy.

51. Anish. “Understanding Sacrificial Anodes on Ship.” Marine Insight, https://www.marineinsight.com/tech/understanding-sacrificial-anodes-on-ships/.

52. “What Is Galvanic Corrosion and How Can It Be Prevented? - TWI.” Joining Innovation with Expertise - TWI, https://www.twi-

global.com/technical-knowledge/faqs/faq-what-is-galvanic-corrosion-and-how-can-it-be-avoided. Accessed 27 Apr. 2024.

53. "Marine Electrolysis & Galvanic Corrosion | City of Kodiak Alaska." Home Page | City of Kodiak Alaska, https://www.city.kodiak.ak.us/ph/page/marine-electrolysis-galvanic-corrosion.

54. Vargel, Christian. "Chapter B.3 - Galvanic Corrosion." Elsevier, 2004, doi: https://doi.org/10.1016/B978-008044495-6/50013-6.

55. Chun Li, WANG, et al. Effect of Temperature on the Galvanic Corrosion of Cu-Ni Alloy/High Strength Steel in Seawater. College of Aerospace and Civil Engineering, Harbin Engineering University Harbin, China, 2016, doi:DOI: 10.1051/matecconf/20166 .

56. Tim Yan,（Titanium Factory). "What Metal Makes the Best Anode?" LinkedIn, 3 Jan. 2024, https://www.linkedin.com/pulse/what-metal-makes-best-anode-tim-yan-titanium-factory--0mytc.

57. "Galvanic Corrosion - SSINA." SSINA, https://www.ssina.com/education/corrosion/galvanic-corrosion/.

58. "Galvanic Corrosion – One of the Biggest Enemies of Boats in the Water | Suenos Azules Marine Surveying and Consulting." Suenos Azules Marine Surveying and Consulting, https://www.facebook.com/WordPress.com https://suenosazulesmarinesurveying.wordpress.com/2012/04/20/galvanic-corrosion-one-of-the-biggest-enemies-of-boats-in-the-water/.

59. Otutu, Michelle. "Impressed Current Cathodic Protection." Corrosionpedia, Corrosionpedia, 25 Oct. 2013 https://www.corrosionpedia.com/definition/impressed-current-cathodic-protection-iccp

60. CORROSION PROTECTION OF SHIPS by Det Norske Veritas (DNV)